POLYMER MATERIALS, PROCESSES, AND STRUCTURES FOR OPTICAL TURNING IN 3D GLASS PHOTONIC INTERPOSERS

A Thesis
Presented to
The Academic Faculty

by

William A. Vis

In Partial Fulfillment
of the Requirements for the Degree
Masters of Science in the
School of Georgia Institute of Technology

Georgia Institute of Technology
May 2016

POLYMER MATERIALS, PROCESSES, AND STRUCTURES

FOR OPTICAL TURNING

IN 3D GLASS PHOTONIC INTERPOSERS

Approved by:

Dr. Rao R. Tummala, Advisor
School of Materials Science and Engineering
Georgia Institute of Technology

Dr. Venkatesh Sundaram
School of Electrical and Computer Engineering
Georgia Institute of Technology

Dr. Dong Qin
School of Materials Science and Engineering
Georgia Institute of Technology

Date Approved: 26 February 2016

Dedicated to Pete and Karen Vis

ACKNOWLEDGEMENTS

First of all, I would like to thank my advisor and committee chair, Professor Rao R. Tummala for his leadership and guidance. Also, I am very thankful for the thorough review and guidance from my mentor and committee member, Dr. Venky Sundaram. Additionally, I am grateful for the technical feedback from my committee member, Professor Dong Qin.

Several industry collaborators made this research possible. I would like to thank Jack Mateosky and Mike Frankel from Ciena Corp. for their funding, characterization support, and technical guidance. I would like to thank Jibin Sun and Terry Bowen from TE Connectivity Ltd for their funding, die support, and technical guidance. I would like to thank Aurélie Mayeux and Amit Ghosh from MicroChem Corp. for supplying LightLink™ and providing technical expertise. I would like to thank Aric Shorey from Corning Inc. for supplying the glass substrates and for drilling through-vias in glass. I would like to thank Byron Lubenkov from Infinte Graphics Inc. (IGI) for supplying high quality glass and Mylar masks. I would also like to offer a big thank you to Ryuta Furuya from USHIO for lithographic support in the double-sided mask fabrication. His expertise enabled high quality alignment.

Several experienced Georgia Tech researchers provided me with invaluable knowledge and support. I am very thankful for the technical guidance in optical fabrication and characterization from Dr. Fuhan Liu and Dr. Daniel Guidotti. I would also like to thank Dr. P. M. Raj for his etching support, Dr. Venessa Smet for her assembly guidance, and Dr. Himani Sharma for her technical guidance in polymer dilution.

I am extremely thankful for the day-to-day help from my team member, Bruce Chou in all aspects of modeling, design, fabrication, and characterization. His passion for photonics and work ethic are an inspiration. Furthermore, I would like to thank the interns in the photonics team, Abhishek Thumaty and Bilal Khan for their day-to-day fabrication and characterization support. I would also like to thank the new team members, Rui Zhang and Sukhadha Viswanathan for their polishing support.

I am very grateful for the support from other members of the PRC family. I would like to thank Chandra Nair and Saumya Ghandi for their sputtering support for mask fabrication. I would like to thank Tim Huang for his AFM characterization support. I would like to thank Brett for his writing support. I would like to thank the visiting engineers, Akira Mieno, Yuya Suzuki, Yutaka Takagi, and Yoichoro Sato for their fabrication instruction when I first joined. I would like to thank Jason Bishop for his help in the experimental holder construction and Chris White for his tool assistance. I would like to thank Karen May, Patricia Allen, Brian McGlade, and Susan Bowman (from the MSE department) for their administrative support. I would like to thank the other interns, Martin Schubert, Tim Fleck, Lukas Schueth, for their day-to-day fabrication support. Lastly, I would like to thank Bhupender, Ninad, Zihan, Kaya, Nathan, Gary, Sri, Sangbeom, Vijay, Dibyajat, Partha, Jialing, and Satomi and for their friendship and memories at PRC.

TABLE OF CONTENTS

Page

LIST OF TABLES

Page

LIST OF FIGURES

Page

SUMMARY

Optical interconnections have been the primary method for long haul data communications for decades due to their very high bandwidth capability beyond copper-based electrical interconnections. There is a growing interest in adopting optical interconnects over distances less than 10 meters, driven by the escalating demand for higher bandwidth in data centers and cloud computing networks. In these applications, optical and electrical integration has been combined primarily at the board-level with optical backplanes coupling to fibers, and discretely packaged photonic and electronic ICs attached to the backplanes by surface mount technology (SMT). Although integration of photonic and electronic functions are beginning to be integrated on single chips called Silicon Photonics, this technology is limited in its ability to integrate into complete systems. The pioneering work on 3D Glass Photonics at Georgia Tech aims to achieve the highest integration density of electrical and photonic interconnections at lowest power consumption and lowest cost, enabled by advances in glass interposers. The objectives of this thesis research are to design, fabricate and demonstrate optical waveguides with integrated turning structures in glass interposers, for delivering light from optical fibers to photonic ICs with lowest transmission loss.

There have been several recent reports on high-density electrical wiring fabrication on glass interposers, and in these, polymer waveguides have been previously demonstrated at board-level. However, this research represents one of the first studies on optical waveguides and turning structures fabrication on thin glass interposers. Also, the processing conditions of polymer waveguides, especially siloxane-based polymers, on glass interposers have not been reported in the literature. Polymer waveguides with ultra-smooth glass as the cladding layer enable much lower optical loss compared to prior work using polymer cladding on both sides of the core. This research also leverages the

optical properties of soda-lime silica, borosilicate, and boro-alumino-silicate glass substrates to demonstrate for the first time, an improved incline lithography method to define integrated 90 degree turning structures at the ends of the polymer waveguides for light turning and coupling to vertical emitting lasers and photodetectors.

In this research, several fundamental materials and process challenges were addressed leading to the demonstration of an optical waveguide with an integrated turning mirror structure with 'self-alignment' in 3D glass interposers. First, the glass-polymer interface was investigated using Atomic Force Microscopy (AFM) and contact angle goniometry. Process guidelines for surface preparation and adhesion enhancement with a siloxane-based polymers were established. Next, the precise lithographic definition of planar waveguides was optimized for multi-mode geometries. To achieve the target height, a two-step spin coating process was developed, after careful optimization of the process steps based on fundamental characterization. For example, the degree of solvent evaporation was quantified using Thermal Gravimetric Analysis (TGA), to optimize the soft bake step.

A new *parallel* process was introduced to enable alignment of the out-of-plane turning structures to pre-existing features, such as electrical pads for photonic die assembly. An immersible carrier was designed with an adjustable tilt and index-matching media to enable this process. The angle tolerance of the micro-mirrors were modeled using Finite Domain Time Difference (FDTD) and Beam Propagation Modeling (BPM). Using the proposed process, three-dimensional siloxane polymer waveguides (3D WGs) were demonstrated on ultra-thin glass substrates – within the modeled angle tolerance. The misalignment of the optical structures to pre-existing features was measured to be an average of ~2.3um across the 100mm x 100mm panel.

CHAPTER 1

INTRODUCTION

In the past four decades, high bandwidth electronics have been driven by the ability to increase transistor density at lower cost as predicted by Moore's Law, which states that the number of transistors per chip doubles approximately every two years. This transistor scaling is expected to run into many fundamental problems including: leakage at front end, RC delays at the back end, and limited cost reduction at the next node. Thus alternative technologies capable of higher data bandwidth per unit of power and cost are needed. Hence Georgia Tech and other groups have been developing "system scaling" technologies, which integrate multiple devices at system level along with passive components, on high density substrates called interposers with highest I/O density.

1.1 Optoelectronics Trend in Cloud Computing and Automotive Applications

Optoelectronic interconnections have the potential to enable system scaling at **higher bandwidth**, **higher power efficiency** and **lower cost** than copper wiring, which suffers from resistive line losses. The bandwidth density (in bits/s) of copper interconnects scales proportionally to cross-sectional area and inversely to the square of distance [1]. Therefore, for **high bandwidth** cloud computing applications, there is a critical distance in which conventional electrical interconnects are surpassed by optical interconnects. Furthermore, as the bandwidth demand increases, that critical distance over which optical interconnections are superior, decreases. This has driven the adoption of optical interconnections from board-to-board [2-4] to chip-to-chip [5-7] and even to intra-chip, as shown in Figure 1.1 [8].

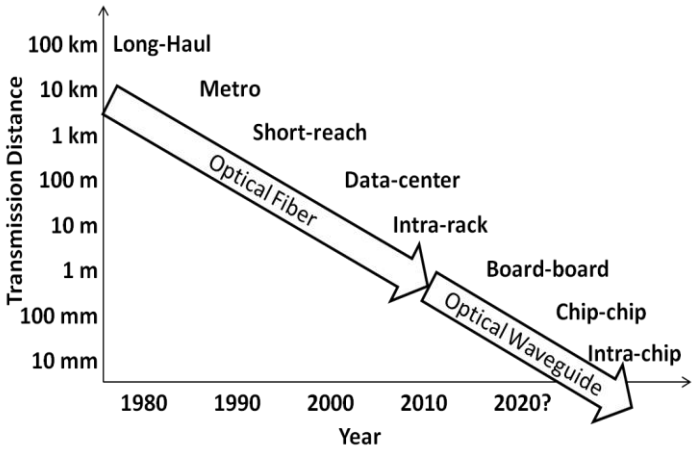

Figure 1.1: Adoption trend for optical interconnections [8]

The higher bandwidth capacity per channel of optical fibers compared to copper wires, has also driven the increasing use of optical fibers for data transfer within automobiles. The new era of automotive electronics, with the highest electronics content in any system, is expected to increase significantly in the next decade, driven by such innovations as autonomous driving, 5G wireless streaming, and all electric drivetrains. The size, weight, and power consumption (SWAP) of copper wires in the car, along with stringent shielding requirements from electromagnetic interference (EMI), have motivated the increasing adoption of optical interconnects in automotive applications.

The two major challenges limiting the expansion of optical interconnections to higher volume applications are power efficiency, quantified as loss (in dBs) and high cost. The typical target for optical line loss is less than 0.05dB/cm. The high cost comes from expensive devices such as compound semiconductor lasers, packaging cost, as well as from the stringent and expensive requirements for active optical alignment at system-level.

1.2 Optoelectronic Interconnections and Packaging Technologies

Fundamentally, an optical link can be broken into three elements: the optical interconnect, source or detection photonic die, and any necessary coupling structures between devices and fibers, including optical turning. Figure 1.2 illustrates the fundamental components of any optical link.

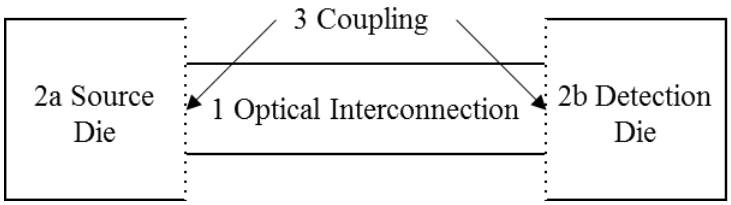

Figure 1.2: Components of an optical link

1.2.1 Optical Interconnections

With the exception of free-space optics, optical interconnections are achieved by an *optical waveguide* that confines a photonic signal by total internal reflection (TIR) – a condition established by an index of refraction difference between an inner higher index core and outer lower index cladding. For longer distances (intra-rack or longer), the optical waveguide is defined by a cylindrical glass fiber. Glass optical fibers are categorized by their modal confinement. Multi-mode fibers (MMFs) have core diameters of 62.5um or 50um and single-mode fibers (SMFs) have core diameters of ~9um. The decreased core diameter of SMFs, 'squeezes out' higher order modes, until a single mode remains. In either case, the fibers have a 125um diameter outer glass cladding. The index of refraction difference between the core and cladding is ~0.05. Figure 1.3 presents the geometry of MMF and SMF core and cladding.

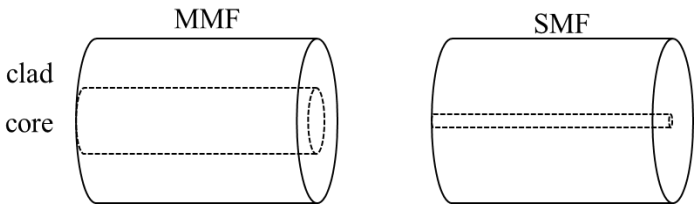

Figure 1.3: Geometry of MMF and SMF core and cladding

In optical fiber coupling to the package or interposer, a fiber holder is usually constructed out-of-plane (vertically) using a through-silicon-via (TSV) [9, 10] or in-plane (horizontally) using a groove [11]. The **in-plane** approach has better mechanical stability as a fiber is mechanically constrained along the fiber length by any allocated distance along the substrate surface (1-15mm). The additional mechanical constraints minimize fiber tilt, a significant contributor to fiber coupling loss. Figure 1.4 presents the typical in-plane fiber integration approach.

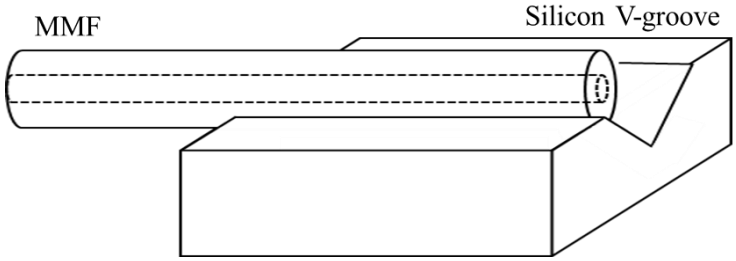

Figure 1.4: Integration of optical fiber-in plane

Within the package or interposer, an optical waveguide carries the light from the fiber as defined by an **in-plane** structure of rectangular cross-section made of polymer, glass, or ceramic material. Due to the size of fibers (MMF and SMF), the waveguides at the package-level are typically of similar dimensions to the fiber cores, albeit of rectangular instead of circular cross-section. Matching the size and confinement conditions is important to minimize fiber to waveguide coupling loss known as mode-mismatch loss. The step-index waveguide structure is a common, simple approach to minimize mode

mismatch loss. Figure 1.5 presents the geometry of multi-mode and single-mode step-index waveguides.

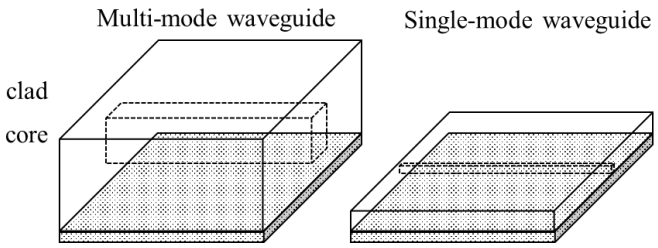

Figure 1.5: Geometry of multi-mode and single-mode waveguide core and cladding

The material for optical waveguides can be polymers, glasses or ceramics. Polymer waveguides are most suited in package or interposers due to their wide range of film thicknesses (5-70 um) and low temperature processing. Polymer optical waveguides are the main focus on this research, and prior work is described in detail in Chapter 2. Multi-mode glass waveguides are also being developed as an embedded approach in glass substrates using novel ion-exchange processes [12]. Although ceramic waveguides with much higher index of refraction are employed with submicron dimensions for on-chip integration [13], they are not suitable for coupling to fibers on interposers.

1.2.2 Coupling to Photonic Dies

Conventional laser photonic dies emit light either in-plane using an edge-emitting laser (EEL) or out-of-plane using a vertical cavity surface emitting laser (VCSEL). The ability for VCSELs to be integrated in an array provides significant scaling advantage to EELs [14]; therefore, the **out-of-plane** transmission is the preferred choice. In light detection, a photodetector detects light in-plane using Si-Ge photodiodes (PDs) or out-of-plane using P-i-N (P-type Intrinsic N-type) photodiodes or metal-semiconductor-metal (MSM) photodiodes. P-i-N PDs have the best performance at the lowest cost, again making **out-of-plane** transmission the preferred choice, as shown in Figure 1.6.

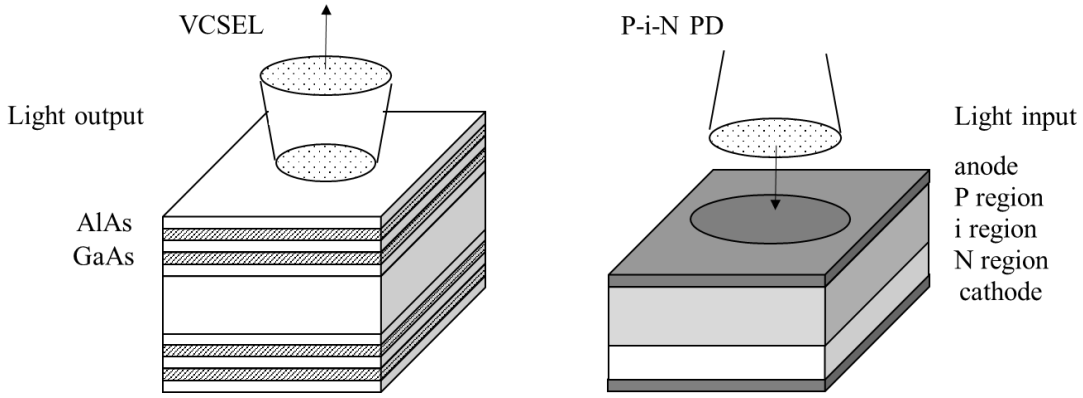

Figure 1.6: Out-of-plane light orientation of VCSEL and P-i-N photodetector

1.2.3 Need for Precise Turning Structures Integrated with Waveguides

Given the advantages associated with out-of-plane light transmission for photonic dies and in-plane light transmission for optical waveguides and fibers, a 90 degree *optical turning structure* is required to complete the optical link, independent of the transmission distance. Figure 1.7 shows the general architecture and an example of such an architecture, namely IBM's board-to-board optical link known as Terabus [2].

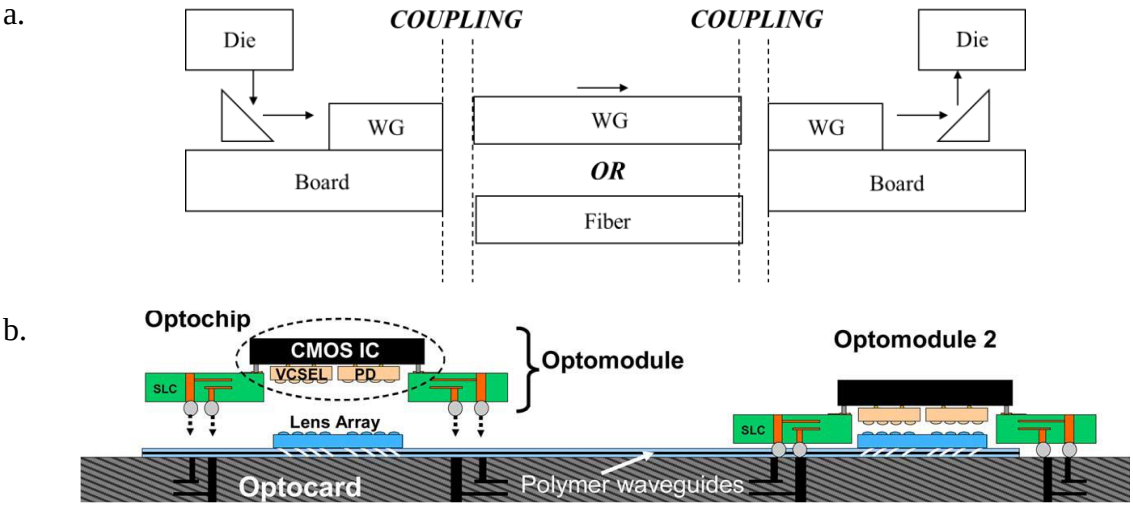

Figure 1.7: Turning architectures: (top) general schematic
(bottom) IBM's Terabus board-level optical link [2]

1.2.4 Need for Optoelectronic Interposers

One of the main challenges associated with optoelectronics at board-level, is the alignment of the photonic ICs to the turning structures. Alignment accuracies, between the active photonic on-chip area and the turning structure, of less than 2 um are required for multi-mode transmission with much smaller offsets of ~0.5 um needed for single-mode, in order to meet the optical loss specifications. This assembly tolerance is difficult to achieve due to the large CTE mismatch between Si (~3ppm/K) or GaAs (~6ppm/K) and conventional FR-4 printed circuit boards (17ppm/K). A common approach is to increase the tolerance using lenses, however this drives up the cost and complexity.

Board-level integration imposes additional limitations on the electrical interconnections, in terms of both signal speed and I/O pitch scaling. A novel architecture, called 3D glass photonic interposer (3DGP) was proposed by Georgia Tech to integrate all the elements of the optical link, including fiber to waveguide coupling structures, waveguides, turning structures, and coupling to photonic ICs. Such an interposer also integrates high I/O density wide bus electrical interconnections as well as high speed electrical signal lines for the best figure of merit (FOM) for bandwidth, power and cost. Such an interposer also improves the accuracy of photonic IC bonding as coefficient of thermal expansion (CTE) matching enables assembly accuracies of less than 0.5um, eliminating the need for lenses.

1.2.5 3D Glass Photonic Interposers

In this thesis, polymer waveguides with self-aligned turning structures are integrated in 3D Glass Photonic Interposers being developed at the Packaging Research Center (PRC), Georgia Tech [15-18], as shown in Figure 1.8. Due to its excellent electrical, optical, and mechanical properties, glass is superior to silicon or organic as the core material for the

interposer substrate [19]. Figure 1.8: 3D glass photonic interposer architecture for chip-to-chip (top) and fiber-to-chip (bottom) interconnections

Table 1.1 presents a comparison between these three substrate materials for photonic and electronic integration.

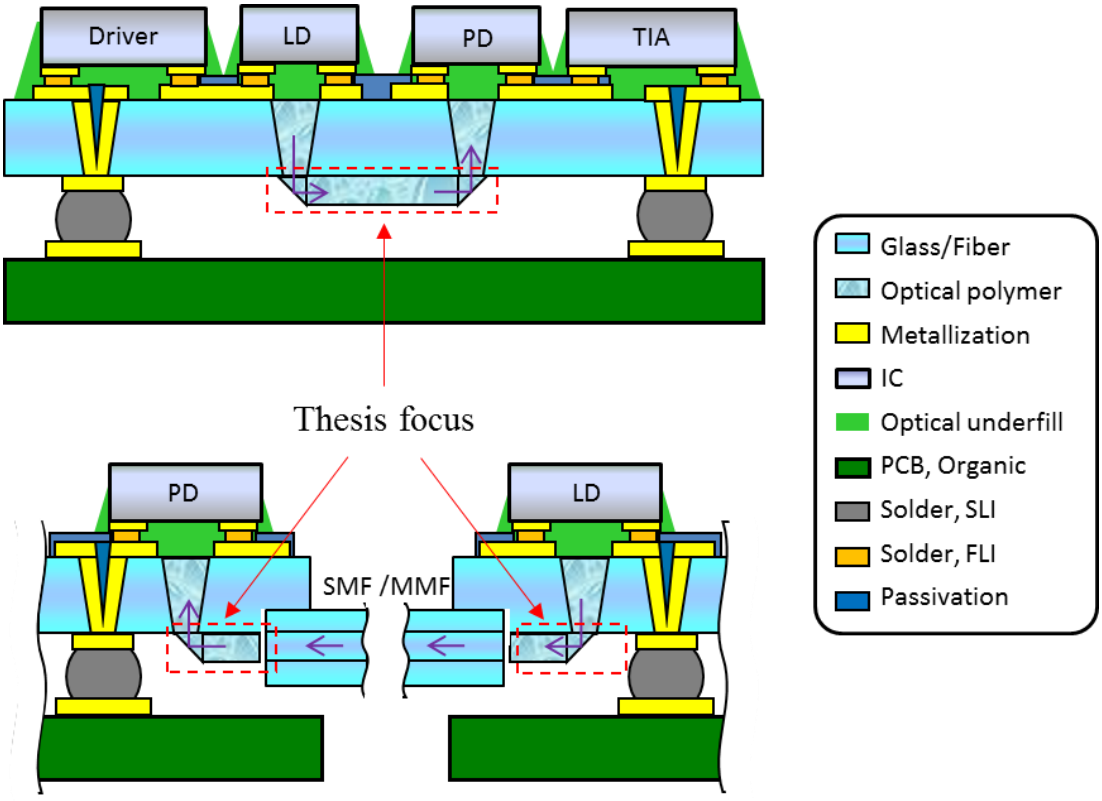

Figure 1.8: 3D glass photonic interposer architecture for chip-to-chip (top) and fiber-to-chip (bottom) interconnections

Table 1.1: Comparison of substrate technologies rated by relative contribution (*, **, and ***) towards objectives for 3D glass photonic interposer

Interposer Objectives Required Properties	**Glass** Soda-lime	**Silicon**	**Organic** FR4
Low loss electrical signaling dielectric constant, ε_r loss tangent, tan δ @ 10 GHz	*** 5-7 0.006	* 11.7 0.015	** 4-4.8 0.009-0.021
Through-substrate optical signaling absorption coeff., α [cm^{-1}] @ 850nm	*** 0.47	** 591	* N/A
Substrate as cladding index of refraction, n @ 850nm	*** *1.52*	* 3.65	* N/A
Low interfacial loss surface roughness, Ra [nm]	*** <1	*** 0.15-0.3	* 300-5800
Fine assembly tolerance coeff. of thermal expansion, CTE [ppm/K]	*** 3-8.5	*** 3	* 17
Dimensional stability Young's modulus, E [GPa]	*** 50-90	*** 130-185	** 21-24
Low cost manufacturing volume [panel or wafer]	*** *panel*	* *wafer*	*** *panel*

For electrical signals, glass has the best properties for high speed transmission, with low dielectric constant and the lowest loss tangent [20]. For optical transmission, the optical transparency across a broad range of wavelengths, low index of refraction, and ultra-smooth surface of glass allow for fabrication of low loss polymer waveguides, which are simpler to fabricate and with lower loss, since the glass substrate can be used as the

bottom cladding layer. Further, glass enables a unique parallel processing technique for fabrication of optical turning structures, described later in this document. The tailorable CTE of glass enables matching to various photonic dies, enabling the fine assembly accuracies needed for low coupling loss. Additionally, glass has better dimensional stability than organic laminates, which is critical for low loss coupling both at the fiber/WG interface and between the turning structure and photonic die. Lastly, glass has the potential for low cost and high throughput manufacturing enabled by large panel processing of optoelectronic modules and lower cost substrate materials and processes.

Polymer waveguides were chosen as the waveguide material in this research, due to their low loss and low temperature, panel processing compatibility. For instance, polymer waveguides can be deposited by dry film lamination, patterned using package-level lithographic techniques, using non-aggressive chemistries (compared to ceramic etchants), and cured at low temperatures (<150C) with no inherent limitation to volume scaling. Chapter 2.1 details the various polymer optical waveguide materials and the specific materials selected for the 3D glass interposers.

1.3 Research Objectives and Challenges

The objective of this research is to demonstrate polymer waveguides with integrated *optical turning structures* in ultra-thin glass interposers, for fiber-to-chip or chip-to-chip optical interconnections, as depicted in Figure 1.9. The key fundamental material and process challenges associated with achieving this objective are labeled in the figure. The unique approaches pursued in this research are to overcome the technical challenges that include: (1) achieving excellent adhesion of polymer waveguides to smooth glass

surfaces, and (2) developing an inclined lithography technique to define the waveguide and turning structure simultaneously and with accurate alignment.

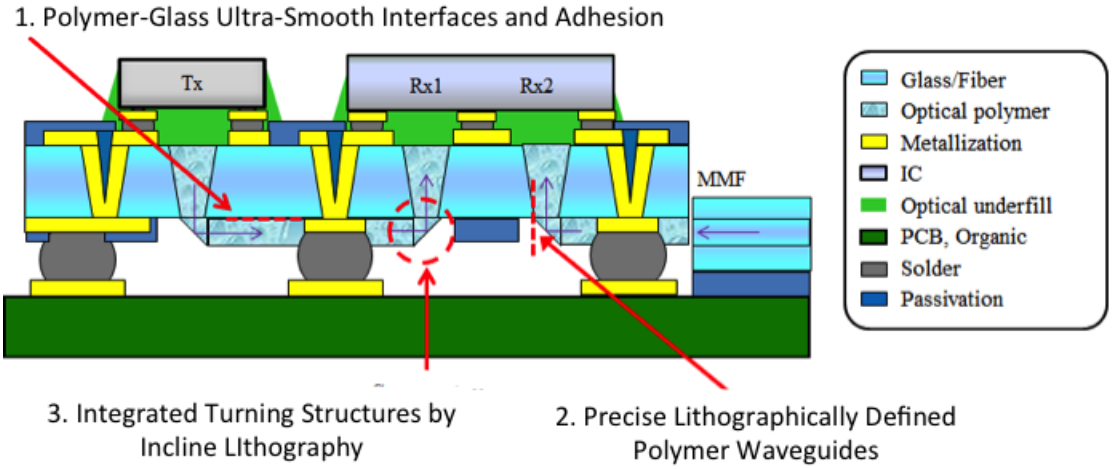

Figure 1.9: Thesis Research Objective and Technical Challenges

The specific objectives, prior art, unique approach beyond the prior art, and technical challenges are summarized in Table 1.2, which forms the basis of the thesis research.

Table 1.2 Thesis Objectives, Unique Approach Beyond Prior Art and Technical Challenges

Parameters	**State-of-the-art**	**Research Objectives**	**Technical Challenges**
Stack-up	Multi-layer	Single layer	Polymer-Glass Ultra-smooth Interface and Adhesion
Alignment	10um	2um	Precise Lithographically Defined Polymer Waveguides
Through-put	10/s	10000/s	Integrated Turning Structures by Incline Lithography

1.4 Research Tasks and Thesis Organization

The research tasks are consistent with the above research objectives of low loss and low cost and are listed below:

Task 1: To study the surface of as-received Corning Willow™ glass and establish process guidelines for surface treatment and adhesion promotion for LightLink™ processing.

Task 2: To design, fabricate, and characterize polymer optical waveguides using LightLink™ on glass substrate with precise height and lithographic definition.

Task 3: To model, design, fabricate, and characterize optical turning structures – namely TIR micro-mirrors – using the proposed novel, modified inclined lithography process, enabling alignment on glass substrate.

This thesis is organized into six chapters. In summary, this chapter reviews the status of optoelectronic technology, the motivation for the proposed research highlighting the benefits of 3D glass photonic interposers, and proposes a novel process for fabrication of the polymer-based optical turning structures. The next chapter provides a detailed review of current commercial polymer waveguide materials, the fabrication of the siloxane waveguides, and an overview of the current processes and structures for optical turning.

Chapter 3 focuses on the first research task, includes a review of the fundamentals of surface analysis, and presents the results for surface treatment and adhesion enhancement. Chapter 4 focuses on second research task, presents the design of experiments to achieve high-quality siloxane waveguides, the optimized results for the individual process steps, and the associated SEM characterization.

Chapter 5 focuses on the third task, presents the modeling of the turning angle tolerance, the design of holder and experiments for the optical turning structure fabrication using the proposed process, the SEM characterization of the turning structures, and lastly the process compatibility of the optical turning structure with pre-existing optical vias. Lastly, Chapter 6 summarizes the results and closes with suggestions for future work.

CHAPTER 2

LITERATURE REVIEW

The objective of this section is to review prior published art in polymer optical waveguide materials, the fundamentals of step-index waveguide fabrication for the selected siloxane polymer, and the structures and processes for out-of-plane optical turning.

2.1 Material Selection for Polymer Waveguide

For any optoelectronic package, a waveguide material is chosen based on its processing and loss characteristics. In regards to processing, a polymer optical waveguide material can first be evaluated by its patterning process. Typical patterning processes for waveguide materials include: UV lithography [21], reactive ion etching (RIE) [22], and laser ablation [23]. UV lithography creates a pattern directly, whereas RIE is a material removing process, therefore additional pre-patterning of a mask on substrate is required. Laser ablation creates a pattern directly, however unlike UV lithography or RIE, the process is serial. Therefore, materials that can be patterned by UV lithography directly are preferred for throughput and process simplicity.

Regardless of processing capabilities, the material of choice must also be low loss. The material loss of an optical polymer is dependent on both intrinsic and extrinsic factors, which can be subdivided further into two mechanisms: absorption and scattering. Intrinsic absorption occurs because of vibration overtones and electron transitions. For

the former, the higher harmonics of the common C-H bond typically occur in the mid-infrared spectrum. For the latter, the presence of conjugated double bonds typically occurs in the UV and visible spectrum. Therefore, there are absorption minimums at the common wavelengths of operation: 850nm, 1310nm, 1550nm. Across all wavelengths, intrinsic scattering occurs due to fluctuations in composition or index of refraction and the presence of local dipoles. All of these scattering sources are of much smaller wavelength than the operating wavelength, therefore they satisfy the Rayleigh criterion. These scattering sources are processing-based and are unavoidable for conventional waveguide processing. Similarly, extrinsic absorption and scattering are associated with the presence of impurities, which are dependent on processing condition. However, these losses can be minimized by careful control of processing conditions. As a result, these losses do not have a characteristic profile. Therefore, the characteristic attenuation profile – the signal loss per distance (dB/cm) vs. wavelength – for a polymer waveguide material is primarily absorption-based. Table 2.1 overviews the potential intrinsic and extrinsic loss in a polymer waveguide.

Table 2.1: Intrinsic and extrinsic loss effects

Intrinsic Absorption	**Intrinsic Scattering**	**Extrinsic Absorption**	**Extrinsic Scattering**
Vibration overtones	Rayleigh scattering	Moisture	Network structure
Electronic transitions		Contaminants	Fabrication defects
			Birefringence
			Cracking

For the proposed glass photonic interposer, the index of refraction also needs to be matched because the glass substrate is being utilized as part of the waveguide stack-up. Also, low temperature processing is important for process compatibility. Processing temperatures can be inferred from the glass transition temperature.

Conventional optical polymers include: polymethyl-methacrylate (PMMA), polystyrene, polycarbonate, polyurethane, epoxies, acrylates, siloxanes, polyimides, and olefins. Companies that develop optical waveguide materials include: Dow Chemical, Dow Corning, Du Point, Hitachi, MicroChem Corp., Mirco Resist Technology GmbH, NTT, and RPO Pty Limited. Table 2.2 shows commercial optical polymers designed for 850nm transition and their parameters for evaluation.

Table 2.2: Types of polymers used as optical waveguides @ 850nm

Supplier	**Type [Trade Name]**	**Process**	**Loss [dB/cm]**	**n @ [nm]**	**T_g [C]**
Dow Corning®	Siloxane [24] [Optical Elastomer]	Laser, UV	0.05	1.54	200
MicroChem Corp	Siloxane [LightLink™] [25]	UV	0.05	1.51	100
MicroChem Corp.	Epoxy Novalak Resin, ENR [26] [SU8]	UV	2	1.59	210
Micro Resist Technology, GmbH	Organically modified ceramics (ORMOCERs) [OrmoCore] [27]	Laser, RIE, UV	0.06	1.52-1.54	250
Micro Resist Technology, GmbH	Epoxy [EpoCore][27]	UV	0.2	1.57	180
RPO Pty Limited	Inorganic polymer glass IPG™ [28]	UV	0.22	1.49-1.54	300

In this research, LightLink™ (LL) – a polysiloxane supplied by MicroChem Corp. is selected [29]. LL is the best candidate for the 3D glass interposer because it can be patterned by UV lithography, has low loss at 850nm, and has an index of refraction similar to the glass substrate. As a bonus, LL can be processed at low thermal conditions (<150 C), adding process compatibility. The rest of the chapter will provide a review of the detailed siloxane polymer process for waveguide fabrication and the associated advanced processing for optical turning structure fabrication.

2.2 Polymer Waveguide Fabrication

Given the requirement for ultra-low loss, polymer waveguides have to be fabricated with very high-quality – more so than their electrical counterparts – whose irregularities in cross-sectional geometry are less performance critical. For multi-mode transmission, the typical geometry of a polymer waveguide is 50um x 50um. For low loss, the waveguide's cross section must be uniform along its length as any irregularities in the height or sidewall offer significant contribution to the overall transmission loss. Therefore process understanding is paramount to ensure high quality, low loss waveguide fabrication. The first area of consideration for any process flow is the substrate and stack up.

2.2.1 Stack-up

Conventionally, polymer waveguides are fabricated as clad-core-clad on polymer. The polymer is either a smoothing buffer layer for a conventional substrate (i.e. FR4) or the substrate itself (i.e. flexible substrates). Figure 2.1 illustrates a characteristic stack-up on a PCB.

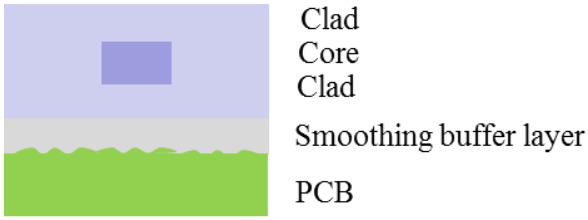

Figure 2.1: Characteristic Waveguide stack-up

2.2.2 Siloxane Polymer Waveguide Fabrication

Siloxane polymer waveguides have been fabricated using conventional UV lithography [21] and even a novel electro-static induced lithographic technique [30]. The standard fabrication process for LightLink™ (LL), introduced and trademarked by Rohm and Haas [25] and supplied by MircoChem [29] can be subdivided into seven fundamental steps:

I. Substrate Preparation

Before fabrication of the core or clad, a sequence of cleaning steps are typically required to ensure the compositional purity of the surface. Next, an adhesion promotor is optionally deposited (by vapor deposition or spin coating) to maintain the cleaned surface and/or modify the surface for increased chemical interaction with the siloxane.

II. Deposition

The siloxane polymer is supplied in a (Propylene glycol methyl ether acetate) PGMEA solution, which acts as a ‘good solvent’ and allows for tailorable viscosity. In solution, the polymer can be deposited by doctor blading (panel-

scalable), inkjet printing (panel-scalable, but serial), and spin coating (wafer only). For doctor blading, the deposition thickness is determined by the blade height and the planarity is determined by viscosity. For spin coating, the deposition thickness is determined by the initial viscosity and subsequent final spin speed. Lower spin speeds (<750rpm) typically result in non-planarity, therefore the solution should be of sufficient low viscosity (achieved by dilution) to achieve the desired thickness at higher spin speeds. Spin coating also has the drawback of edge-bead formation – a local increase in polymer thickness at the wafer edge – due to surface tension effects.

III. Soft Bake

A soft bake is the first thermal input to the polymer system and typically occurs below the curing (hard bake) temperature. The purpose of the soft bake is to remove the solvent used for deposition. Soft bake also affects cracking, lithographic resolution, and hardness [31].

IV. UV Exposure

UV exposure is the basis of any photolithographic process used in microelectronics. The irradiated UV light defines a local region of crosslinking (for negative-tone) dictated by a mask. There are a variety of lithographic tools developed for this form of pattern transfer.

V. Post Exposure Bake (PEB)

For negative tone polymers such as LightLink™, the material exposed by UV irradiation begins to cross-link or polymerize due to the formation of a photo-acid, which acts as a catalyst. The mobility of the photo-acid is limited at room temperature, therefore an optional post exposure delay can be performed to allow for sufficient time for polymerization with limited diffusivity into unexposed regions. Polymerization is slow at room temperature, therefore a post exposure bake can be performed. At higher temperatures, the rate of polymerization will increase, unfortunately along with mobility of the photo-acid. Diffusion as a result of the higher temperature can occur into unexposed regions.

VI. Development

After irradiation, the local regions of material inhomogeneity are exploited for pattern generation by wet etching or 'development'. Specifically, the non-cross-linked polymer has increased solubility which enables dissolution in a solution, specifically a basic solution (NaOH).

VII. Cure

The siloxane polymer is a thermoset, therefore upon sufficient thermal activation (i.e. 'curing'), the polymer will form an insoluble 3D network of cross-linked covalent bonds. This condensation reaction results in a rapid increase in viscosity until a gelation point in which the polymer chains are no longer dissolvable. The degree of crosslinking known as the degree of cure (D.O.C) can be measured

using Differential Scanning Colorimetry (DSC). There is a saturation point of complete vitrification. For end use application, 100% DOC is preferred, however less than 100% DOC is useful for further sequential processing (i.e. additional polymer core or clad layer adhesion). The optimization of siloxane curing for reliability has been demonstrated [32].

2.3 Optical Turning Structures

2.3.1 Diffraction gratings

Optical beam turning has been achieved using diffraction gratings [10, 33, 34] or micro-mirrors. For this research, diffraction gratings were not pursued due to the need for feature sizes less than the wavelength of the patterning light, which is currently only achievable using expensive wafer-based technologies like e-beam lithography [10, 33] or non-standard photolithographic methods like interference lithography [34, 35].

2.3.2 Mirrors

There are two mechanisms for optical turning using mirrors: 1) reflection – typically metallic and 2) total internal reflection (TIR), established by a sufficient index of refraction difference from one material to another, for a given angle defined by Snell's Law. For either mechanism, as with other electronic components, there are two approaches to fabrication: discrete or integrated.

There are many techniques for *discrete* 45° micro-mirror fabrication, such as polishing [36], ultra-precision machining (UPM) [3], deep proton writing [37], and inclined

lithography [38, 39]. After fabrication, the discrete mirror can be assembled by bonding [36] or insertion [3, 37]; or transferred by molding or embossing [38, 39]. The discrete approach has advantages, namely in quality assurance as the mirror can be inspected before being committed to the next stage. However, the drawback is that the integration challenge is shifted to a secondary step, which may not meet the precise assembly requirements. For example, Jeong et al proposed a low cost solution using a mechanical alignment jig which enabled alignment tolerances of ±10um for a PDMS mold [40]. However, the tolerance is one order of magnitude too large, and while it may be improved, feasibility at panel-scale has yet to be demonstrated.

There are also techniques to fabricate *integrated* micro-mirrors, that is to say, the micro-mirrors are fabricated directly in the application substrate with no additional integration step. In this case, integration (in regards to alignment) is achieved during the fabrication step. While this approach requires that quality be tightly controlled as the mirror is committed up-front, the overall process flow is simpler as no secondary assembly process is required. The two most common techniques are subtractive in nature; they include laser ablation [41] and dicing. While these techniques have been demonstrated for low turning loss, they are inherently limited in throughput due to their serial nature.

Research has been undertaken to develop integrated micro-mirrors using advanced, parallel photolithographic techniques, which include: gradient exposure techniques (i.e. shadow mask [42], grey scale mask [9, 42] , and moving mask [43]) and inclined lithography. Due to challenges in alignment, inclined lithography was categorized as a

discrete mirror fabrication method. However, the process proposed in Chapter 5.2 addresses that challenge.

For the grey scale method, a gradient pattern is fabricated on the mask by stippling. The gradient pattern correlates to a gradient exposure which can be translated into the photosensitive polymer – *if* the photosensitive material can be developed linearly with respect to exposure. That is to say, for a given time in a development solution, the material removed (or depth of material remaining) is linearly proportional to the exposure received. This requires both additional expense in mask fabrication and development in materials for the desired linear development vs. exposure response. Similarly for the moving mask method, a gradient exposure is translated into the polymer by moving the substrate and mask with respect to each other during exposure. In this case, the development is shifted from tool capability in mask fabrication to tool capability in lithography, and again, a unique material response is required. For either method, positive-tone materials are the only tone-type reported, indicating further limitation in material availability.

Inclined lithography is a method in which the substrate and exposure source are angled with respect to one another. Usually, the substrate rather than the exposure source is more easily angled or ‘inclined’, which establishes the name. Unlike the previous methods, negative- or positive-tone materials can be used and no unique material response is required. However, inclined lithography has its own challenges.

1) An index matching material is required during exposure. While this can be achieved by immersion in glycerol or water, this adds process complexity and often an unfavorable environment for the optical polymer, especially before any cross-linking has been initiated.
2) The mask gap effects that can lead to shape disorientation in conventional planar lithography are even more detrimental to shape generation in the inclined case [44]. X. Lin et al overcome this by fabricating the waveguide structure on the mask itself, yet this presents new challenges in the subsequent molding step [45].
3) The inclined process generates asymmetrical structures, requiring multiple exposures to reestablish a desired symmetry.
4) The primary challenge for inclined lithography for waveguide applications is alignment. While many authors have fabricated the necessary structure, alignment of the structure to a pre-existing feature (i.e. a pad for photonic die assembly) – which is essential for a low loss optical link, has not been addressed.
5) The photolithographic sidewall control is even more critical for optical turning mirrors as the sidewall generated in the planar case will become the inclined, optical turning surface.

2.4 Research Gaps in Existing Body of Literature

As discussed in previous chapters, the development of photonic structures at the interposer-level is in its infancy. While commercial optical waveguide materials have been developed for board-level, there are several important research gaps in development of these materials for application in a 3D glass photonic interposer as outlined below.

1. A thorough analysis of the surface of the soda-lime-silica Willow™ glass being developed by Corning for display technology and eventually interposer/substrate packaging technology – in terms of intrinsic surface properties and equilibrium state (i.e. degree and type of adsorbates) in standard environment (room temperature and atmospheric pressure).

2. Requirements of the Willow™ glass surface – in terms of required cleaning and optional surface modification – for LightLink™ (LL) siloxane polymer adhesion and sidewall control.

3. A relation between soft bake – in regards to heating ramp and maximum isothermal temperature – on extent of solvent evaporation *and* stress at the glass-interposer interface for LL sidewall control.

4. An inclined lithography process within the required alignment tolerances (<2um) for low-loss, polymer-based optical turning structures, namely total internal reflection (TIR) micro-mirrors

CHAPTER 3

INTERFACE AND ADHESION

3.1 Glass as Cladding

Polymer waveguides are typically fabricated as clad-core-clad on organic substrate, such as FR4. As FR4 is a composite material made of a glass fiber weave and an epoxy resin, the surface of FR4 is characterized by waviness. A smoothing, intermediate build-up layer is required to reduce the FR4 roughness for optical applications. Polymer waveguides have also been fabricated on polymer-based flexible substrates [30]. For either case, an additional optical cladding layer is required to establish the appropriate index of refraction and optical transparency for optical transmission.

In this work, the ultra-smooth, transparent glass substrate was used as the cladding layer, instead of the conventional thick-film polymer cladding (and smoothing buffer layer). As a result, fewer processing steps are required, reducing process complexity and subsequently cost. Further, by removing the cladding layer, the electrically superior glass substrate can more easily be accessed for electrical fabrication down the line. This enables reduction in required build-up layers and ultimately form factor. Figure 3.1 presents an example of build-up layer reduction and decrease in form factor with the proposed approach vs. the state-of-the-art.

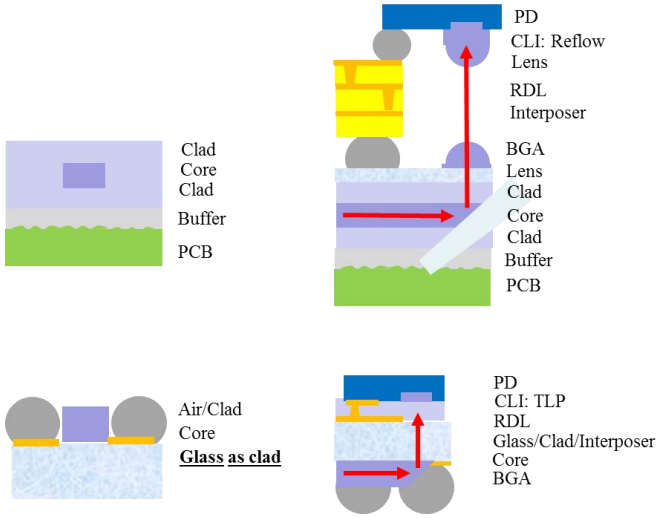

Figure 3.1: Reduction of build-up layers and smaller form-factor:
(top) optical integration on board (bottom) optical integration on 3D glass interposer

Unfortunately, core fabrication on glass introduced challenges in adhesion. For conventional stack-ups, the critical interface for waveguide adhesion occurs between the optical cladding layer and the other polymer. The mechanism for adhesion for these polymer-polymer interfaces is diffusion. In this work, the critical interface for waveguide adhesion occurs between the optical core layer and a glass substrate. Figure 3.2 illustrates the interface of focus. As discussed in the previous section, there is a gap in literature regarding the material's surface and the required processing for waveguide fabrication with good adhesion and sidewall control, leading to the first research task:

Task 1: To characterize the surface of as-received Corning Willow™ glass and establish process guidelines for surface treatment and adhesion promotion for LightLight™ waveguide fabrication.

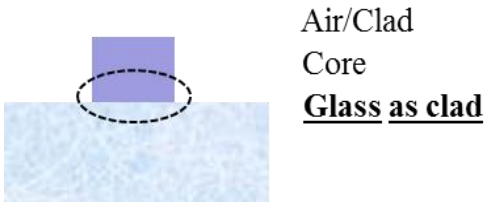

Figure 3.2: Novel polymer waveguide stack-up using glass as clad

3.2 Surface Analysis of Glass

Surface analysis was used to characterize the polymer-glass interface. A material's surface, whose definition is set by atomic or molecular length scales (0-10nm), has properties different than the material's bulk properties. For this research, there were two main parameters examined to define the glass surface: surface morphology and surface energy. Surface morphology is a purely physical parameter that quantifies the geometry of the surface. Conversely, surface energy is chemical in nature and defines the thermodynamic state and chemical composition of the surface, respectively. The energy of a surface, known as the surface free energy, is the energy of the broken / dangling bonds – which exist due to the unviability of bulk atoms.

The surface morphology of the glass substrate can be characterized using Atomic Force Microscopy (AFM), which can provide averaged height information as well as phase irregularities across a representative area. This information is critical in understanding the eventual waveguide adhesion in regards to uniformity and type. The panel-based end-use application for the fabricated polymer waveguides demands adhesion uniformity not only for individual coupons, but across the entire panel (up to 510mm x 510mm).

Further, as adhesion has both physical and chemical components, the extent of physical contribution is useful to understand the total adhesion. AFM was performed on Corning Willow glass [46], a soda-lime silica to be used as the 3D glass interposer substrate. Table 3.1 shows the AFM height data of the glass substrate for a 1um x 1um representative area and Figure 3.3 shows the associated graphic.

Table 3.1: AFM height data of glass substrate for a 1um x 1um representative area

Parameter	**Values [nm]**
Average	-0.0084
Minimum	-5.7129
Maximum	6.2635
Median	-0.0157
Ra	1.1268
Rms	1.4392

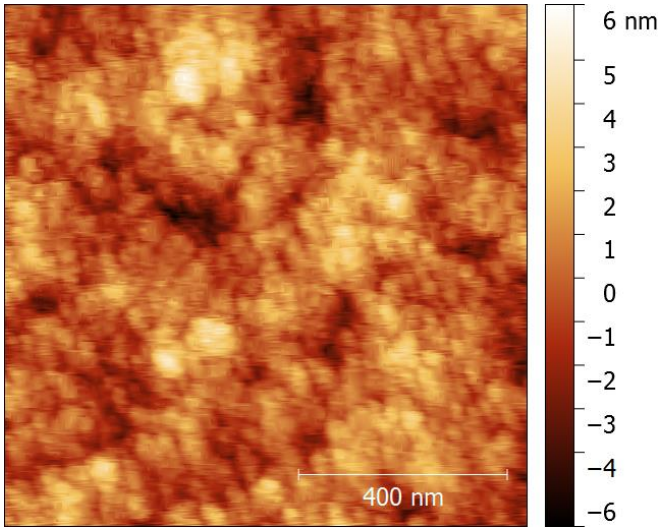

Figure 3.3: Graphical depiction of AFM height data

The quantified, extremely smooth (Ra ~ 1.12 nm) glass surface indicates that physical adhesion of polymer coatings will be minimal.

The surface energy of the glass substrate can be characterized by contact angle goniometry. The energy of the surface dictates the wetting behavior of the polymer in solution and any adhesion promotor on the glass surface. A lower contact angle is an indication of improved wetting. By wetting the surface, the high energy interface is removed. As a result, the contact angle can be used to infer some information regarding the purity of the glass surface. For high energy surfaces like glass, standard environmental conditions (atmospheric, room temperature) will result in some degree of water absorption, oxidation, or any other adsorbate contamination. This is characterized by an increased contact angle.

3.3 Surface Treatment of Glass

Three common cleaning surface treatments were evaluated to ensure a pure glass substrate: acetone/IPA, sonication, and acid piranha. For the acetone/IPA case, the glass was sequentially rinsed with acetone, then IPA, followed by D.I water. Next, the glass substrate was baked on a hotplate for 5 min at 145C to ensure dehydration. For the sonication, the glass was immersed in an ultra-sonic bath filled with alkaline cleaner for 5 min at 50C. Next, the glass was rinsed and dehydrated. For the acid piranha, the glass was immersed in a 3:1 solution of sulfuric acid and hydrogen peroxide for 5 min. Again, the glass was rinsed and dehydrated.

Contact angle measurements were taken on the glass surface using water. An increased contact angle was observed for the acetone/IPA case indicating the presence of residual solvent. Sonication and acid piranha etching resulted in the lowest contact angle.

However as acid piranha etching requires aggressive chemistries, sonication was selected as the process of record (POR) cleaning method.

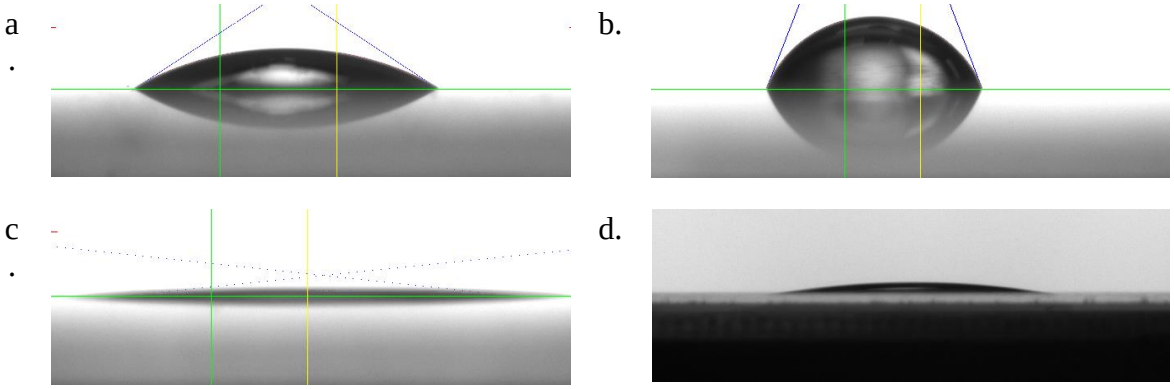

Figure 3.4: Contact angle measurements: (a) as-received, (b) acetone and IPA, (c) alkaline sonication, (d) acid piranha

3.4 Adhesion Enhancement

The cross-section of waveguides fabricated on glass with different adhesion enhancments were characterized by SEM. The full waveguide process is to be discussed in detail in the next chapter. Various degrees of undercutting – an indication of inadequate adhesion – were observed for untreated glass, plasma etched glass, HMDS treated glass, and polymer coated glass. Figure 3.5 shows a comparison between the various adhesion enhancement trials.

The selected time for plasma treatment under standard conditions was limited to 2 minutes by design to avoid introducing additional interfacial loss. Table 3.2 presents the parameters for plasma etching. While additional time increased the roughness and

physical adhesion, the tradeoff for increased loss is not acceptable. A chemical approach was required to address this challenge.

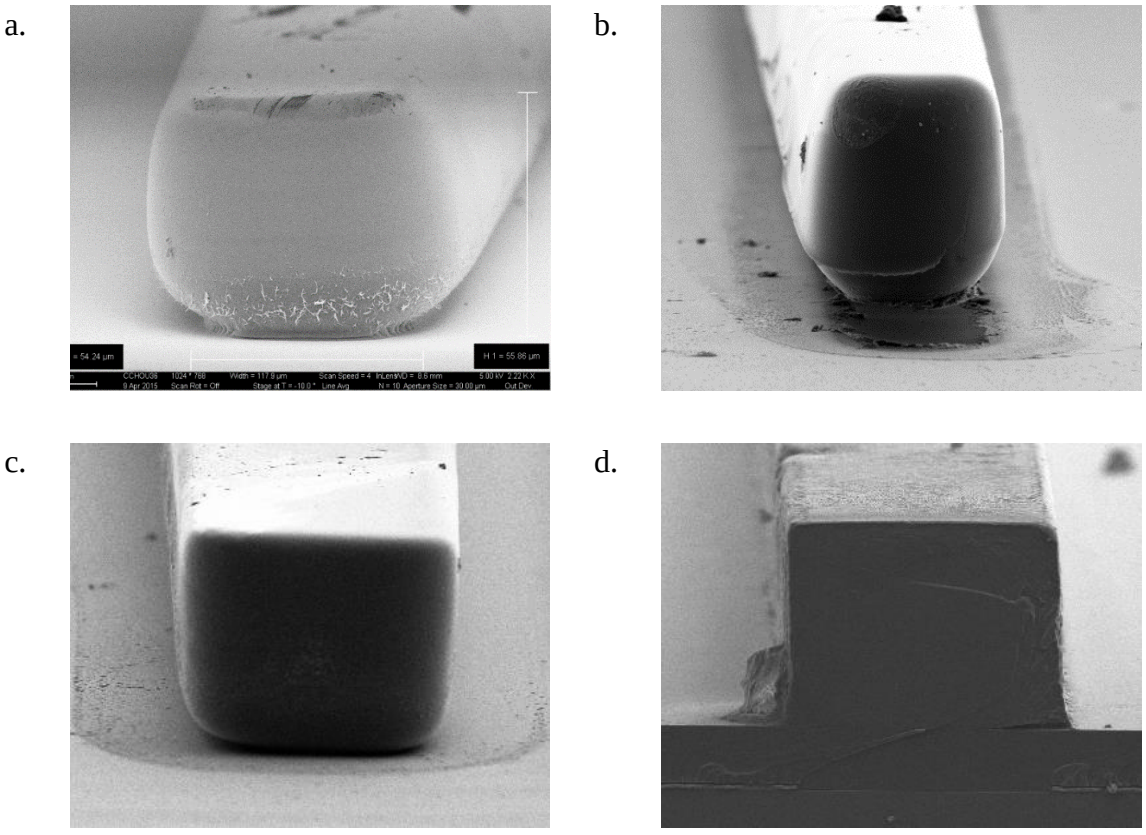

Figure 3.5: Waveguide cross-sections imaged by SEM of various adhesion enhancement: (a) no treatment, (b) oxygen plasma, (c) HMDS, and (d) LightLink™ intermediate

Table 3.2: Parameters for plasma etching

Variable	**Parameter**
Gas	oxygen
Pressure	0.07 Torr
Flow rate	100 sccm
Temperature	100 C
Power	RF 400 Watts
Time	2 min

Minimal undercutting was observed for the HMDS treated glass and the polymer coated glass. For the HMDS treated glass, bond formation was expected between the coupling agent and siloxane polymer due to the displacement of water molecules and generation of trimethylsiloxy groups. However, between the coupling agent and the glass substrate, less H-passivated Si bond formers were available, that is, relative to the conventional Si application. Nonetheless, good adhesion was observed across the 4x4 panel and a 90% yield was demonstrated. For the polymer coated glass, the waveguide material itself was selected to enable self-adhesion eliminating CTE mismatch, ensuring adequate availability of bond formers, and introducing similar surface energies. While the polymer coating does not satisfy the first objective to use the glass as cladding, it does establish the ideal case for waveguide adhesion for comparison and confirm the relationship between adhesion and undercutting. Ultimately, HMDS was selected as the process of record (POR) adhesion enhancer for Corning Willow™ glass.

CHAPTER 4

WAVEGUIDE FABRICAION ON GLASS

As discussed in Chapter 2.2.2, siloxane waveguides have been fabricated using UV photolithography. However, in the prior art documenting LightLink™ (LL) waveguide fabrication, the substrate was not glass. In fact in most cases, the substrate is irrelevant as the process for the optical waveguide core fabrication was sequential to the fabrication of a well-adhered cladding layer of a similar material composition.

In this work, the process for the waveguide *core* fabrication was sequential to the sonicated, HMDS treated glass as described in previous chapter. Figure 4.1 illustrates the intended waveguide geometry. As described in Chapter 2.4, there was a gap in the literature regarding the processing conditions for LL on glass substrate, especially regarding the thermal processing for precise lithographic definition, leading to the second research task:

Task 2: To design, fabricate, and characterize polymer optical waveguides using LL on glass substrate with precise height and lithographic definition

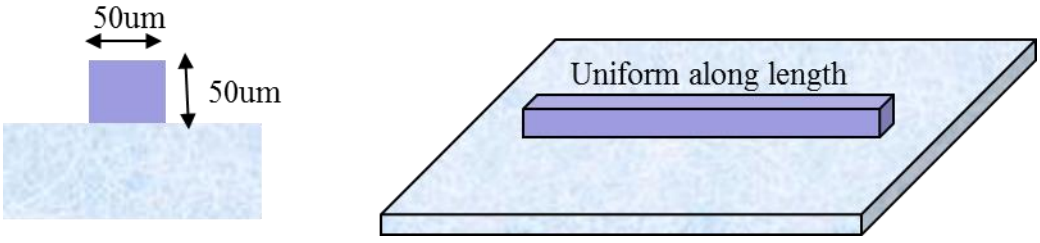

Figure 4.1: Geometric objective for LightLink™ waveguides on glass substrate

4.1 Design of Process

A double spin coat lithographic process was designed to demonstrate siloxane step-index waveguides on glass substrate with precise (±2 um) multimode dimension (50um x 50um) with cross-sectional uniformity with respect to length. Figure 4.2 illustrates the process flow and Table 4.1 presents the detailed steps and parameters.

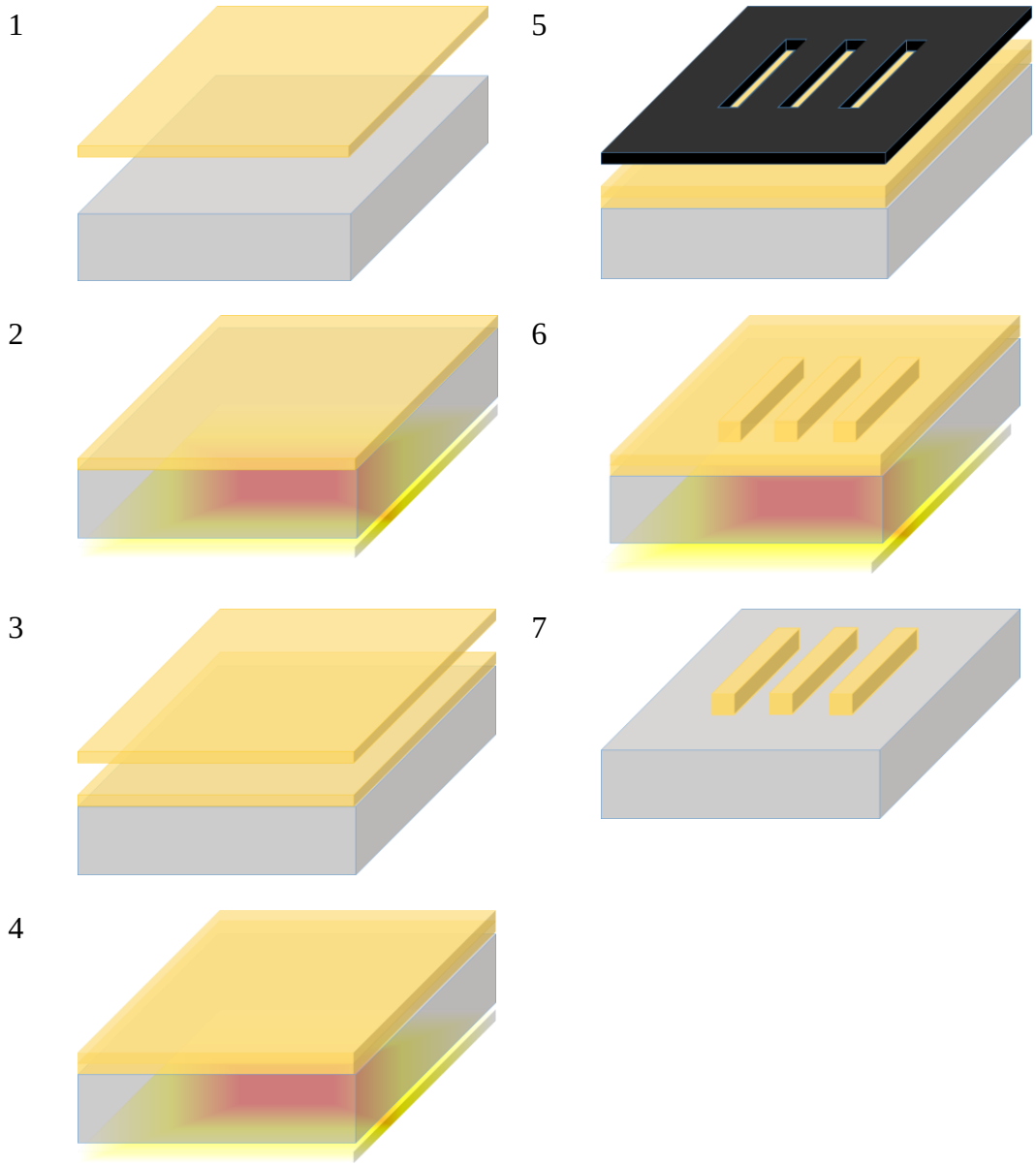

Figure 4.2: Process flow for polymer waveguide fabrication

Table 4.1: Detailed process steps and parameters for polymer waveguide fabrication

Process Step	Type	Parameters
0 Substrate preparation	Surface treatment Adhesion enhancement	Alkaline sonication 80% PGMEA, 20% HMDS
1 Polymer deposition	Spin coating	100 rpm/s 650 rpm, 30 sec
2 Soft bake	Hot plate	90 °C 2, minutes
3 Polymer deposition	Spin coating	100 rpm/s 650 rpm, 30 sec
4 Soft bake	Hot plate	90 °C, 2 minutes; 30 °C/s; 135 °C, 14 minutes
5 UV lithography	I-line	400 mJ/cm
6 Post exposure bake	Delay	25 °C, 15 min
	Hot plate	90 °C, 2 min
7 Development & Cure	Agitated immersion	25 °C, 3 min 45 sec
	Nitrogen oven	145 °C, 60 min

4.2 Process Optimization

The precision of the planar waveguide geometry is paramount. As outlined in the introduction, the dB loss of the optical interconnection or coupling structure is one of the primary objectives for technology adoption. As detailed in Chapter 2.1, much of the total loss derives from extrinsic factors introduced during processing. For the proposed process, the waveguide sidewall becomes the turning mirror surface. Therefore, the sidewall quality is even more critical. As a result, the objective of this section is to fundamentally break down each process step and highlight the methodology for optimization.

4.2.1 Deposition and Height Control

Spin coating was selected as the deposition process. While this common deposition technique is not compatible with large panel processing, it was suitable for process development. For a panel-level application, doctor blading can be interchanged for similar result and ±1.5 um height tolerance as demonstrated [25]. The programmable spin coater used for process development is depicted in Figure 4.3.

Figure 4.3: Experimental spin coater

Fundamentally, spin coating can be broken into four steps: deposition, spin-up, spin-off, and evaporation [47]. Deposition can occur through various means: as an elevated area distribution, as a bolus at the center, as a continuous stream at the center, as a continuous stream from a radially moving port. In either case, the deposition can be performed dynamically or statically. For this work, the deposition was performed statically as a bolus at the center until the radial spreading covers roughly 75% of the substrate.

The second stage is the spin-up, for which the substrate is accelerated to the final, desired, rotation speed. At this stage, the deposited material spreads radially to cover the substrate. The selected ramp speed is less critical. It must be low enough to prevent the substrate from being removed from the vacuum chuck. The third stage is the spin-off. This is the most critical stage. In this stage, the fluid is gradually thinned and uniformity is established. The final thickness vs. maximum spin speed is typically reported for maximum spin speed. Figure 4.4 shows a characteristic height vs. spin speed profile. This profile is dependent on viscosity. In the fourth stage, evaporation of the solvent occurs.

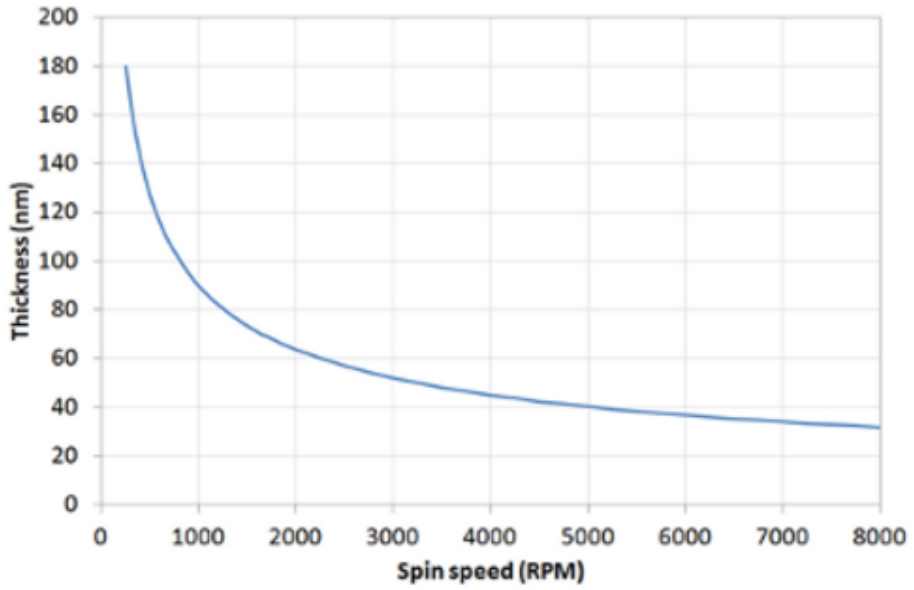

Figure 4.4: Characteristic final thickness vs. maximum spin speed profile

In this work, the viscosity of the polymer (~130 cP) prevented a polymer thickness of 50um at any spin speed. Therefore, two layers were deposited sequentially at 650 rpm with a ramp of 100 rpm/s. The first layer was soft baked on hot plate at 90 °C for 5 min followed by the second layer, which was soft baked on a hot plate at 90 °C for 5 min.

However, for the second layer, the heating was less efficient as the first layer insulated some of the heat. This caused inequivalent thermal input, which resulted in inequivalent lithographic definition. Figure 4.5 illustrates the inequivalent layers observed during the development of the double spin coat process to achieve 50um. Further optimization of the thermal processing was required.

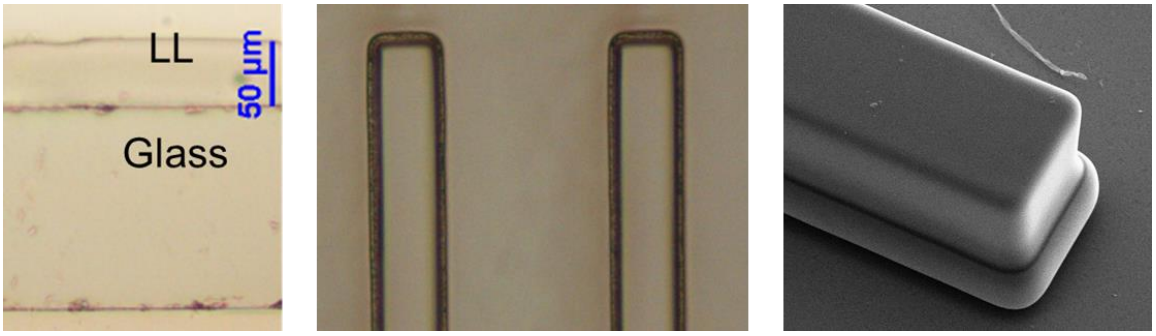

Figure 4.5: Achieving 50um height using the double spin coat process:
(left) cross-section, (middle) aerial optical image, (right) SEM

4.2.2 Soft Baking and Thermal Characterization

As supplied, LightLink™ dissolved in a PGMEA solvent to enable minimal viscosity for deposition. However, adequate evaporation of this solvent is necessary for precise lithographic definition [31]. Additionally, as demonstrated in the previous section, equivalent thermal inputs were required to address the inhomogeneity introduced by two spin coats. Thermogravimetric analysis can be used to quantify solvent evaporation. Three 10 mg samples of LightLink™ were prepared and analyzed using a dynamic scan of 5 °C /min from room temperature to 200 °C by a TA50. Figure 4.6 presents the measured weight percent vs. temperature of one sample. The entire weight loss of ~29% is attributed to the solvent evaporation.

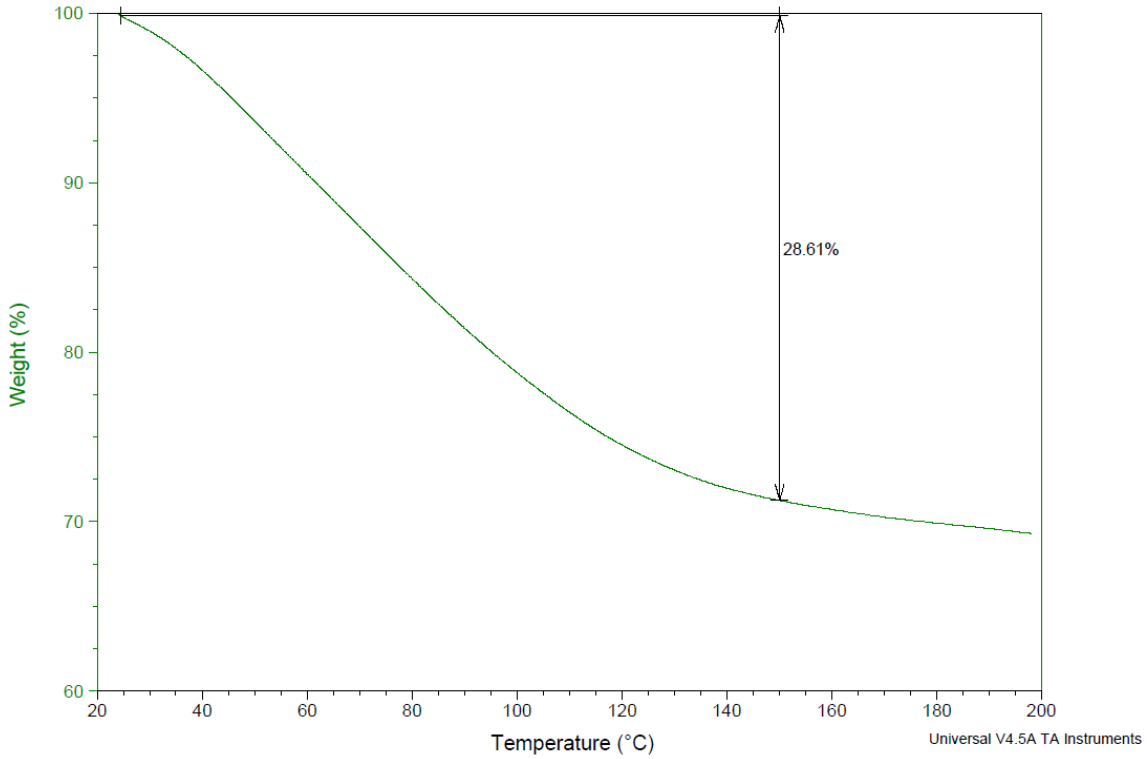

Figure 4.6: Weight percent vs. Temperature of LightLink™ measured by a TA50

The weight percent was used to establish equivalent soft baking thermal inputs. The weights of glass spin coated with LightLink™ were measured before and after soft baking. One fourth of the total weight percent loss (7.25%) was targeted for the first layer and the full 29% was targeted for the second. For the first layer, the isothermal hot plate temperature was kept at 90 °C and the time was adjusted in increments of 30 seconds until the weight percent loss matched the target. For the second, the isothermal hot plate temperature was kept at 90 °C for the first minute then ramped (~30 °C/min) to 135 °C and the time was adjusted in increments of 1 minute until the weight percent loss was matched. Figure 4.7 presents the homogenization of the two spin coat layers imaged by SEM. The final soft bakes for each layer were 90 °C for 2 minutes and 90 °C for 1 min

then 135 °C for 14 minutes, respectively. Further optimization of the exposure, post exposure bake, and development were required to ensure an optically planar sidewall.

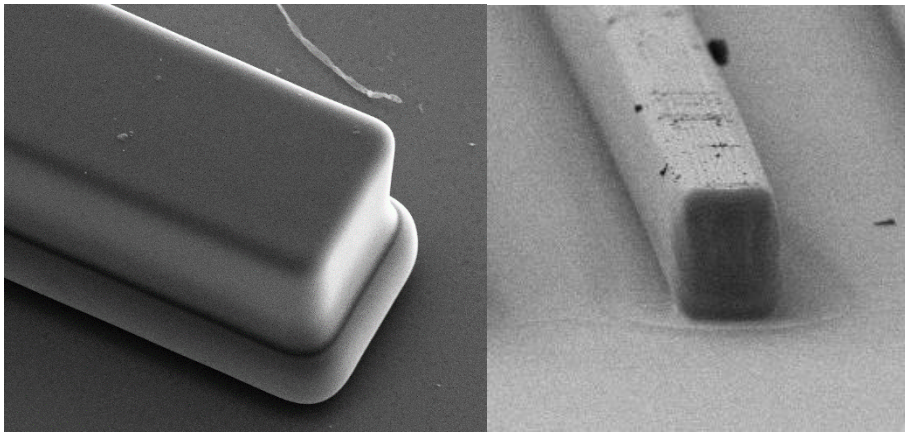

Figure 4.7: Homogenization of double spin coat layers using weight percent loss: (left) before (right) after

4.2.3 Exposure and Post Exposure Bake

As discussed in Chapter 2.1, LightLink™ was selected in part for its compatibility for patterning by UV lithography. As a negative toned material when the polymer is exposed to UV irradiation, cross-linking is initiated. More specifically, a strong acid with absorption near i-line (365 nm) is broken down by the UV light. The acid then catalyzes a condensation reaction wherein two hydroxyl groups are condensed to crosslink two polymer moieties [48]. Water is produced as a byproduct. Figure 4.8 depicts the formation of the high stable Si-O-Si bond.

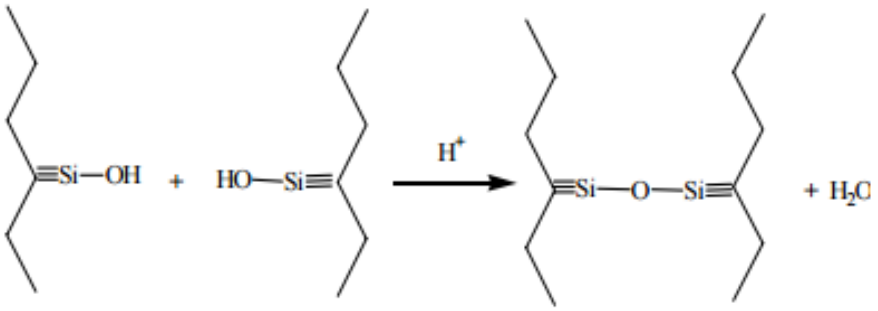

Figure 4.8: Silanol condensation reaction [48]

As the required exposure is dependent on the soft bake condition, multiple exposure 'ladders' were performed during the process development. An exposure ladder is a trial in which the exposure intensity is incrementally increased spatially across the sample. Unlike thickness and baking optimization, multiple data points can be taken using an exposure ladder in one process cycle. Figure 4.9 presents the results of an exposure ladder using a Tamarack mask aligner.

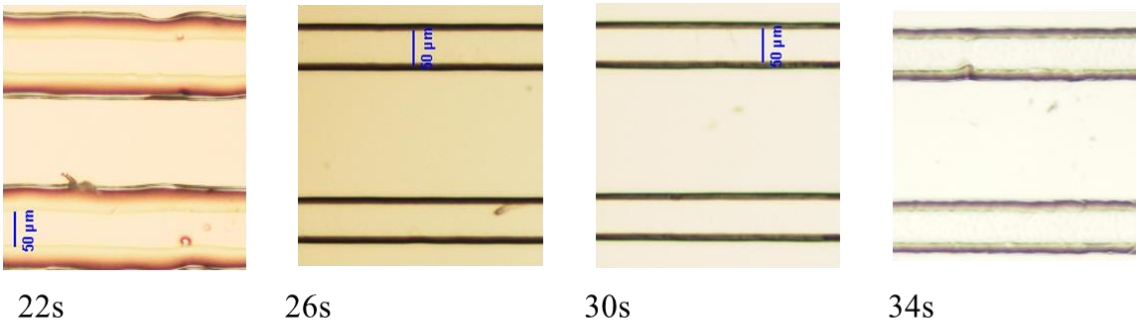

Figure 4.9: Example of exposure ladder using Tamarack mask aligner

Once the condensation reaction has been initiated, the reaction is driven by a post exposure bake (PEB). The purpose of the post exposure bake is to enable sufficient crosslinking for insolubility in a developer. An insufficient post exposure bake can result

in development of both unexposed and exposed regions. However, an excessive post exposure bake can result in bulging of the sidewall as the photo-acid diffuses past the boundary defined by the UV light. A post exposure delay can also be implemented as the reaction will proceed at room temperature with limited thermal activity for acid mobility (i.e. minimal bulging and slow reaction speeds).

In this work, a fifteen minute post exposure delay was selected. Then, an isothermal hot plate baking at 90 °C was performed for which the time was increased from 1 minute to 10 minutes. Development of the exposed region was observed for the 1 minute case, and bulging was observed for the 3 to 10 minute cases. Figure 4.10 illustrates the observed bulging for the most extreme condition (10 minutes) and the ideal sidewall for the 2 minute case.

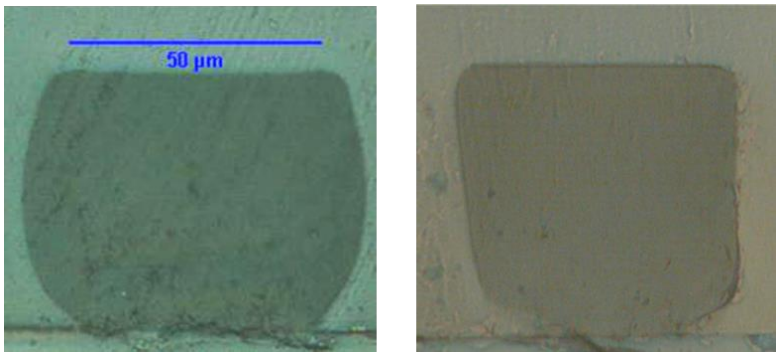

Figure 4.10: Post exposure bake optimization at 90 °C on hot plate:
(left) 10 minutes (right) 2 minutes

4.2.4 Development and Curing

The siloxane polymer is designed for development in an aqueous solution of 0.7N NaOH at temperatures ranging from 21 °C to 37°C by immersion or spray [48]. The eligibility

for development in a relatively non-aggressive chemistry is another advantage of the siloxane polymer. During development, the unexposed region is dissolved. The region exposed is rendered insoluble by the crosslinked structure. Therefore, it remains. The optimal development condition is based on the film thickness, temperature, time, and availability of developer.

In this work, three methods for optimal development were pursued: double puddle, sonication, and immersion. Figure 4.11 presents the characteristic cross-section for each development method imaged by SEM.

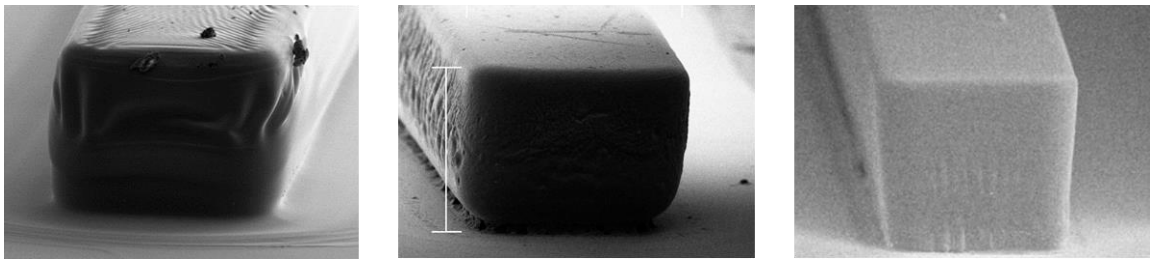

Figure 4.11 Comparison of development methods for optically planar sidewall: (left) double puddle (middle) sonication (right) immersion

For the double puddle process, the developer was heated to 40 °C. For the first puddle, the sample was completely covered with developer for 30 seconds, then dumped. Immediately after the sample was again completely covered with fresh developer for 20 seconds, then dumped. After the second puddle, the sample was thoroughly rinsed in DI water. Inconsistent development was observed across the panel. In some areas, the material between the waveguides was not removed indicating underdevelopment. In other

areas, waveguide delamination occurred indicating over development. In most cases, a wrinkled sidewall was observed.

For the sonication process, the sample was submerged in a room temperature ultra-sonic bath of developer for 5 minutes. In this case, severe waveguide delamination (~50%) was observed. Further, a periodic wave structure was observed in the sidewall. The wave-like structure may be a result of standing waves.

For the immersion process, the sample was submerged in a room temperature beaker of developer for 5 min. A magnetic stirrer was introduced and activated on the lowest setting. Again delamination was observed, indicating over development. However, the time was reduced until no delamination was observed. For a final process of record (POR), a time of 3 min and 45 seconds resulted in no delamination with minimal undercutting and consistency across the 4 in x 4 in panel. The cross-section for the reduced time is presented in Figure 4.11.

4.2.5 Lithographic Definition

The geometry of a representative waveguide cross section with a target of 50 um x 60 um was measured to be 53.96 um x 61.96 um using SEM. Further, the delamination was minimal, and 95% yield was observed. Figure 4.12 presents the measured waveguide and the panel aerial view.

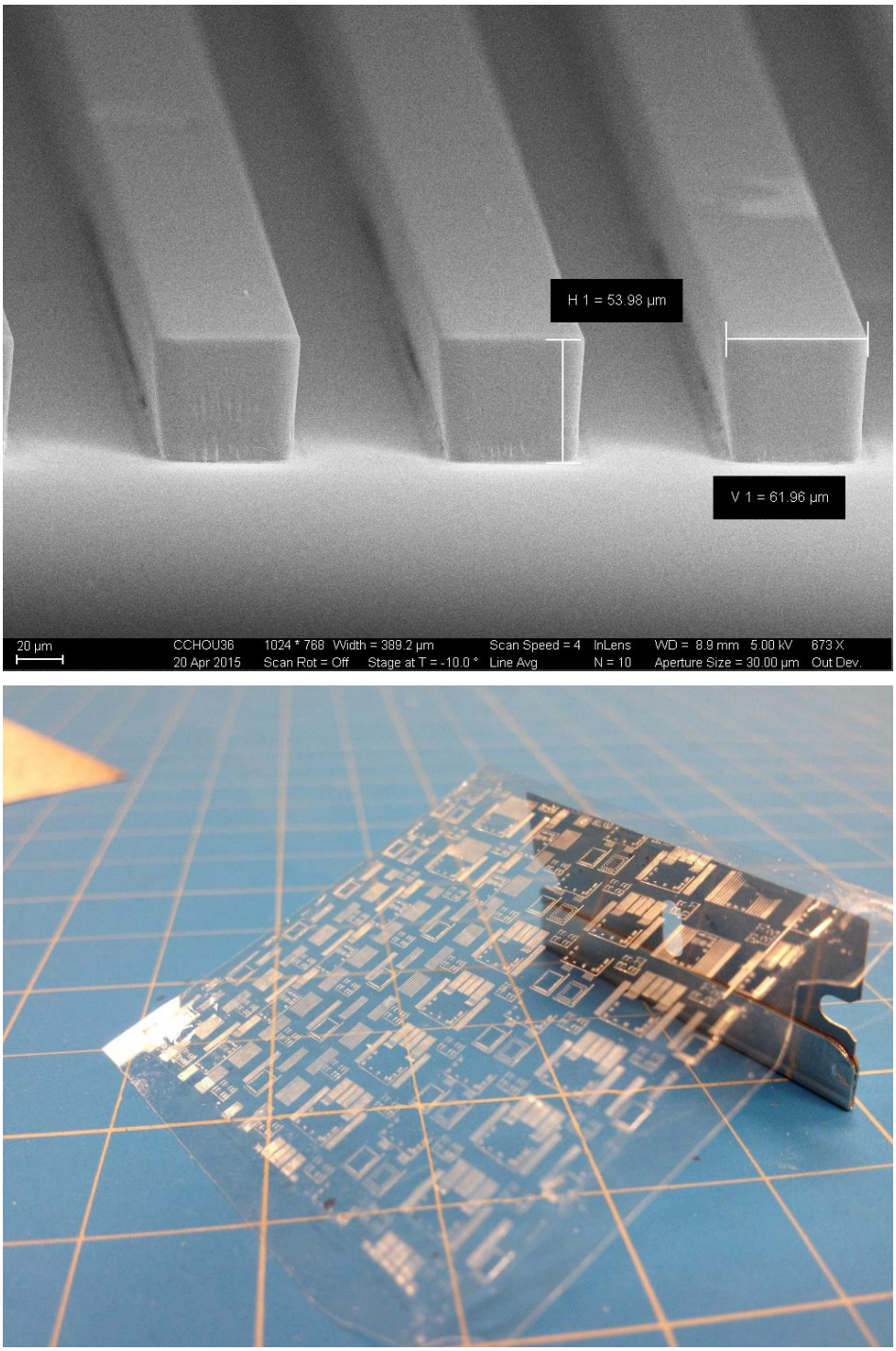

Figure 4.12: Siloxane waveguide using optimized process
(left) cross-section (right) panel view

CHAPTER 5

OUT-OF-PLANE OPTICAL TURNING STRUCTURES

5.1 Inclined lithography

In order to reduce cost, the optical turning structure is fabricated using large-panel lithographic processing. Among them, the TIR micro-mirror fabricated by inclined lithography has the best potential to address the research challenges. There are currently two approaches to inclined lithography: direct integration by top-down exposure and indirect integration by bottom-side exposure. Figure 5.1 presents the representative ray behaviors for each inclined lithography approach. The former has challenges associated with mask shifting during exposure and poor mask contact. The latter requires a secondary transfer step, like molding. Both of these approaches result in poor location alignment, which increases loss due to misalignment between fiber and waveguide or turning structure and photodiode.

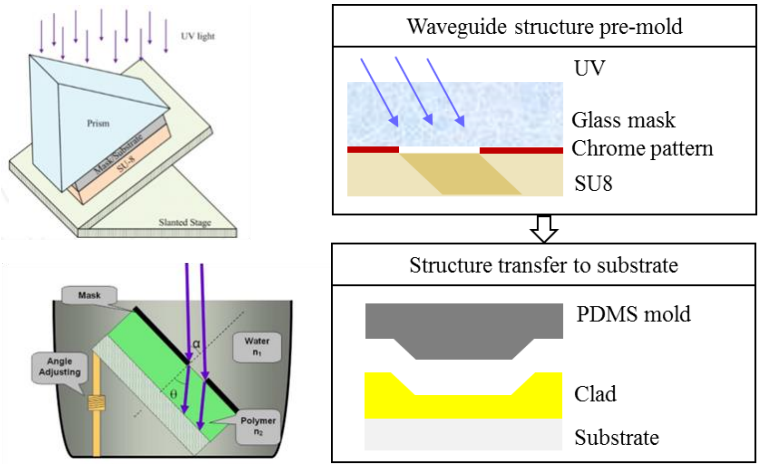

Figure 5.1: Overview of existing inclined lithography approaches: (left) top-down exposure (right) bottom-side exposure and molding

5.2 Modified Inclined Lithography

A novel, modified inclined lithography technique is proposed to improve the alignment beyond the state-of-the-art. Figure 5.2 illustrates the alignment improvement of the process. In the proposed process, metallic masks are fabricated on both sides of the glass substrate using precise, planar lithography. These masks define apertures during inclined exposure, which in turn, precisely dictate the locations of the optical turning structures.

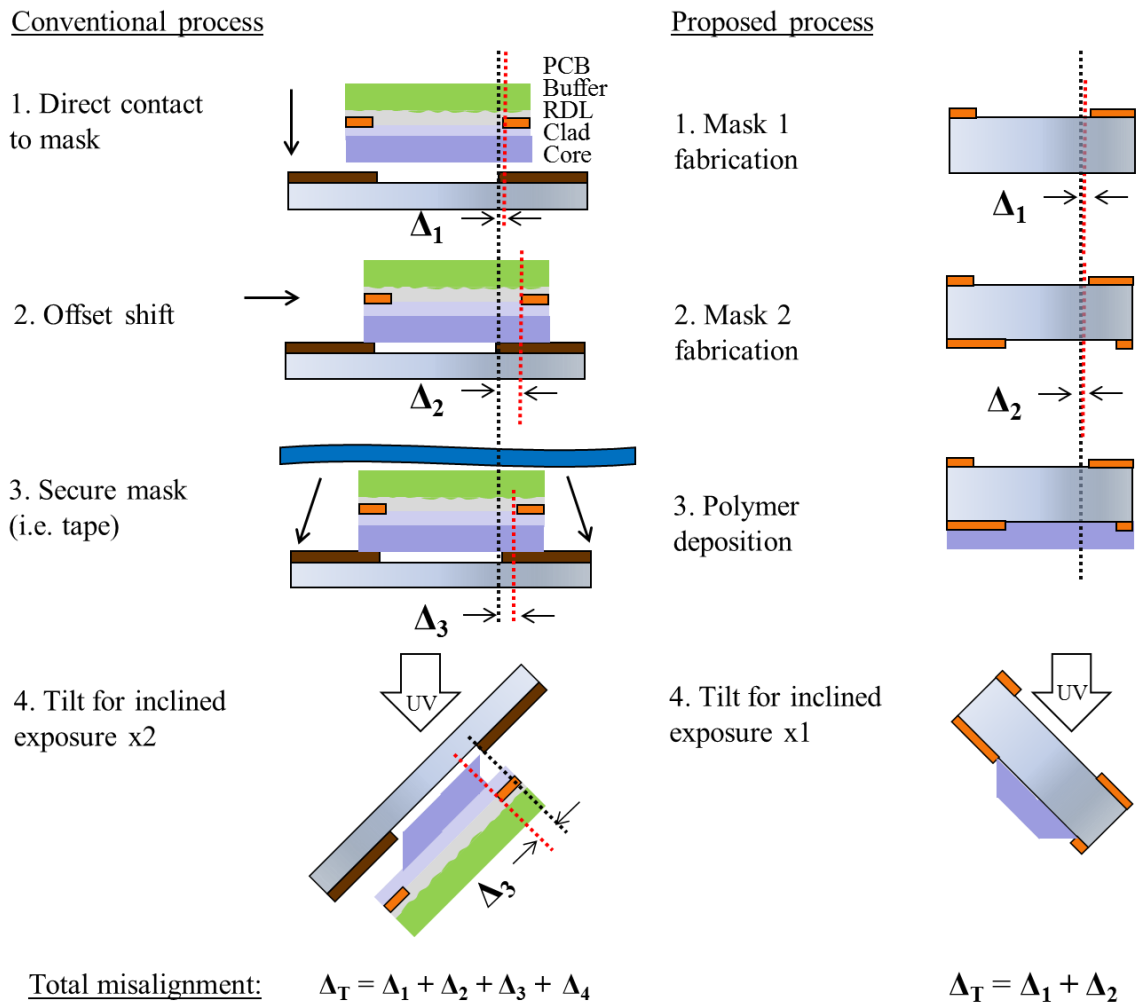

Figure 5.2: Alignment improvement of unique approach vs. state-of-the-art

For the conventional process, the electrical pads for die assembly and eventually light input/output location are aligned to a discrete waveguide mask. Some misalignment, Δ_1 is expected. Next, the sample and mask must be offset to accommodate the tilt. While this offset can be accounted for ahead of time using an offset fiducial, the waveguide thickness variation will directly translate to misalignment, Δ_2. Next, the sample and mask must be secured, contributing to a third misalignment, Δ_3. Lastly, the two must not shift after being secured, contributing to a fourth misalignment, Δ_4.

For the proposed process, the masks cannot shift or have poor contact and no secondary transfer step is required, eliminating the current inclined lithography alignment challenge. The optical waveguide and integrated turning structure are *self-aligned* to the pre-existing direct-coated masks.

Inclined lithography has two other challenges, which are also addressed by the modified process. First of all, a 45° turning angle cannot be formed using inclined lithography outright. Index-matching, specifically immersion in water (n = 1.33 at 365nm) is selected to address the challenge due to its simplicity and panel-level scalability. The second challenge is in symmetry. Inclined exposure generates a rhomboid shaped cross-section with a single exposure. A second exposure can be used to create the turning mirror in the other direction. For the proposed process, a TIR interface is established by reintroducing the air medium and symmetry is established by reflection with one exposure. Figure 5.3 presents the concept of the process, specifically the ray behavior during inclined exposure.

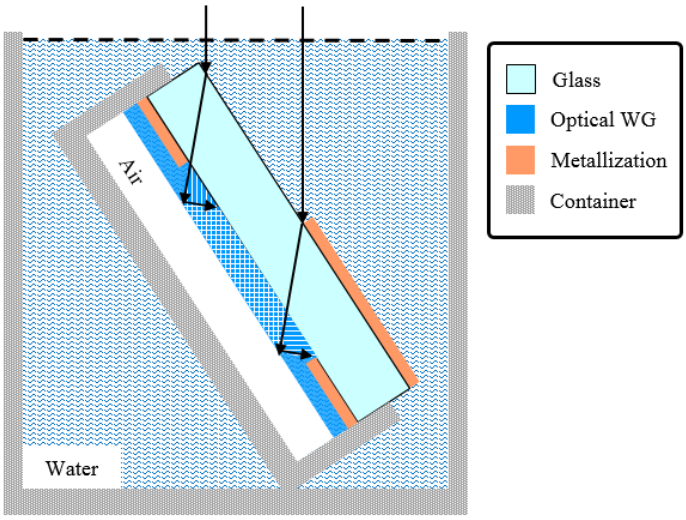

Figure 5.3: Snapshot of ray behavior during exposure in novel incline lithography process

Ideally, all optical turning structures are defined with symmetry using a single exposure. Again, the reduction in process steps infers reduced cost. Figure 5.4 illustrates the geometry of the intended out-of-plane optical turning structure after development. The unique stack-up and process leads to the third task:

Task 3: To model, design, fabricate, and characterize optical turning structures – namely TIR micro-mirrors – using the proposed novel, modified inclined lithography process *enabling alignment* on glass substrate.

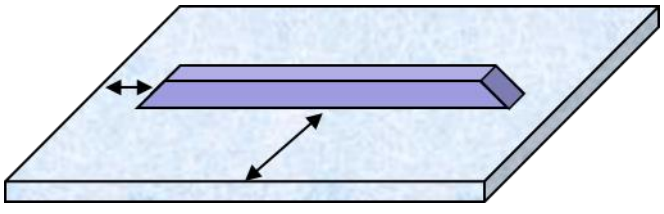

Figure 5.4: Geometric objective for LightLink™ out-of-plane turning structures

5.3 Modeling of Turning Angle Tolerance

Optical loss can be modeled using beam propagation method (BPM), 2D finite difference time domain (2D FDTD) method, and 3D finite difference time domain (3D FDTD) method. However as with any modeling, there is a tradeoff for each method between accuracy and computing demand.

In this work, all three methods were pursued and evaluated for the 3D WG application. That is to say, a 3D WG being coupled into an optical via in glass substrate. An optical via is a through-glass-via filled with the same polymer waveguide material. An optical via can reduce through-substrate loss [15].

Table 5.1 presents a comparison between the three methods.

Table 5.1: Comparison of modeling approaches for optical turning

Method	BPM	2D FDTD	3D FDTD
Accuracy	Low	Medium	High
Memory	<100MB	~ 1 GB	> 50G
Results	Unable to capture	Suitable	Unable to compute

For the approach employing BPM, the memory requirement was very low (<100MB). The optical set up included: a source, 30 um of dispersion transmitted through index-matching fluid (n = 1.50), a 100 um glass substrate (n = 1.50) with an optical via with ~88° taper (n = 1.51), and a turning mirror integrated into a 50um waveguide (n = 1.51) with air as cladding (n = 1). The turning was the primary variable. Figure 5.5 presents the BPM results at three angles: 40°, 45°, and 50°. However, BPM was unable to effectively capture optical turning as the TIR condition is not effectively established.

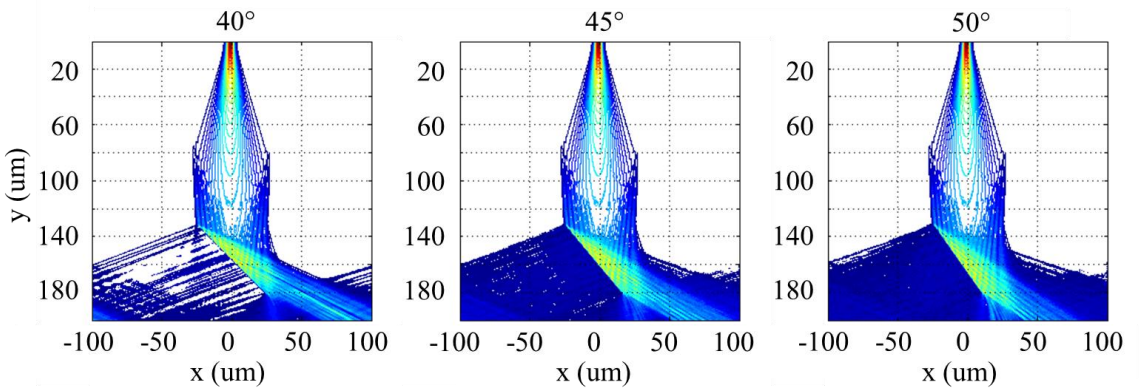

Figure 5.5: BPM results of turning for glass with optical via at various angles: (left) 40° (middle) 45° and (right) 50°

For the approach employing 3D FDTD, the memory requirement was very large (>50 GB). Figure 5.6 presents the geometry of the most accurate modeling case. Unfortunately, 3D FDTD was unable to compute due to the excess number of unit cells. However, for the two-dimensional case, the memory requirement was acceptable (~1 GB) and turning was effectively captured. As a result, a more thorough analysis was performed to evaluate the turning angle tolerance.

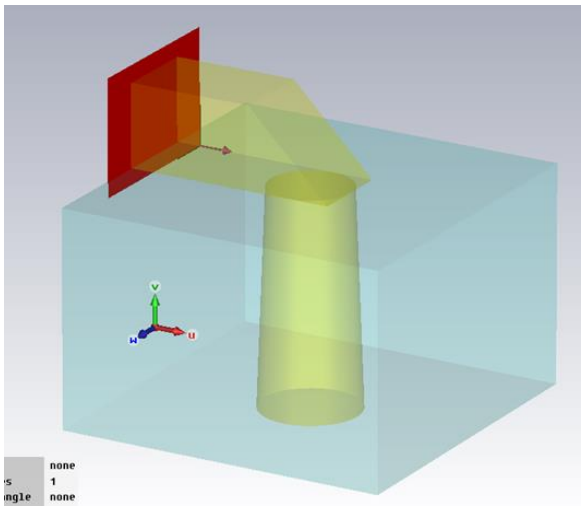

Figure 5.6 Geometry for 3D FDTD modeling

Two setups were pursued to evaluate the minimum and maximum allowable turning angles for 0.5 dB loss, namely with optical via and without optical via. Table 5.2 presents the parameters for each setup. The glass thickness (h) was 130um, the waveguide thickness (w) was 50um, the via diameter (d) was 50um, the turning angle (θ) was varied from 40° to 55°, and the operating wavelength (λ) was 850nm. The optical material properties were also selected for the operating wavelength. Figure 5.7 presents the 2D FDTD modeling results for the setup.

Table 5.2: 2D FDTM setup for turning angle tolerance

With via	Without via	Parameters
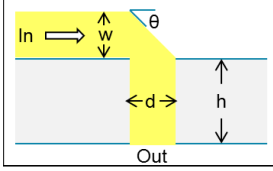	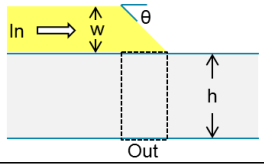	h = 130 um w = 50 um d = 50 um θ = 40° ~ 55° λ = 850 nm

For either case, the modeling results indicated a higher angle tolerance with a negative deviation from 45°. For instance for the 40° case, the turning efficiency was reduced and *some* leakage occurred. For this case, the TIR condition was maintained. However for the 50° case, the turning efficiency was much worse and *significant* signal leakage occurred. This was because the condition for TIR was not maintained. Comparing the two setups, the modeling results indicated a higher angle tolerance for the optical via case. For the case *without via*, the turning angle range for 0.5dB loss was between 43 and 46 degrees. For the case *with via*, the turning angle range for 0.5dB loss was between 42 and 47 degrees. These results indicated that the optical via recaptured signal leakage caused by

turning. Regardless, the lower angle tolerance was selected as a target for process demonstration.

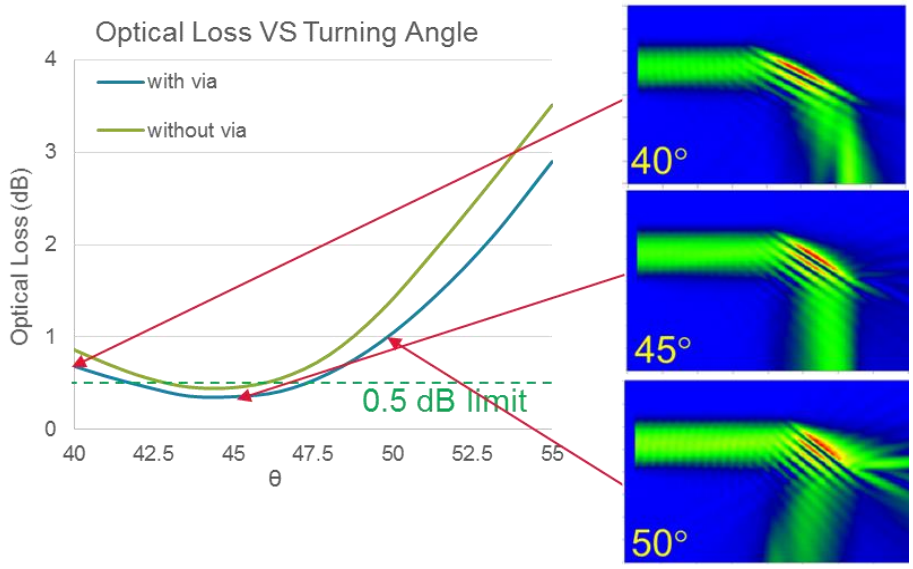

Figure 5.7: 2D FDTD modeling results of turning angle tolerance

5.4 Design of Process

The optimized two-step spin coat process presented in Chapter 4.2 forms the basis for the inclined lithography process flow. In the waveguide case, a discrete mask defined the polymer structure using planar lithography. However in this case, double-sided masks (fabricated directly on the glass substrate) define the polymer structure using inclined lithography. A process flow was designed to enable fabrication of double sided copper masks with precise front-to-back alignment and a calculated **offset** between front-side and back-side mask openings. Further, a holder was designed to introduce the required mediums for a 45° degree turning angle and a reflective interface for symmetry.

5.4.1 Ray Analysis

Ray analysis was used to calculate the required tilt, required offset between mask openings, and confirm the TIR condition for reflection establishing symmetry. The refraction behavior of the rays is quantified by Snell's Law given by:

$$n_i \sin\theta_i = n_r \sin\theta_r \tag{5.1}$$

where n_i is the refractive index of the incident medium, θ_i is the incident angle, n_r is the refractive index of the refracting medium, and θ_i is the refracted angle. Figure 5.8 presents a graphical representation of the ray behavior and the variable assignments for calculations.

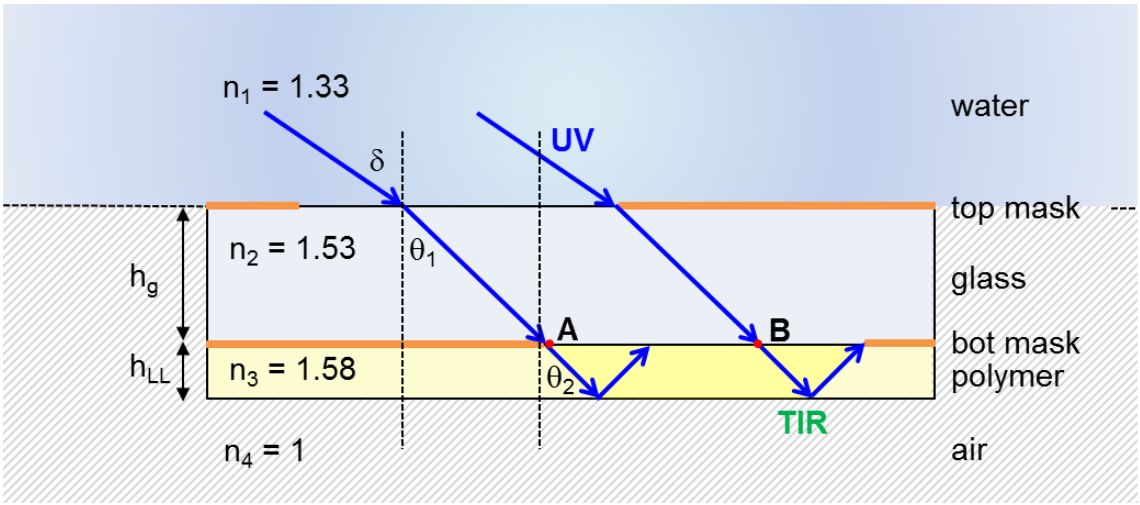

Figure 5.8: Ray analysis during exposure

Rearranging for the modified inclined exposure set up, the tilt is given by:

$$\delta = \sin^{-1}(\frac{n_3}{n_1}\sin\theta_2) \tag{5.2}$$

where θ_2 is the desired turning angle, n_3 is the refractive index of the waveguide material, and n_1 is the refractive index of water. The index of refractions at i-line exposure (λ = 850nm) are n_3 = 1.577 and n_1 = 1.33. Therefore, for a desired turning angle θ_1 = 45°, a tilt of ~57° is required. Similarly, the offset can be calculated by:

$$offset = h_g \tan\theta_1 + 2h_{LL}\tan\theta_2 \tag{5.3}$$

where h_g is the thickness of glass substrate, h_{LL} is the height of waveguide, and n_2 is the refractive index of the glass substrate. The index of refraction for the Corning glass substrate at i-line exposure is n_2 = 1.529. Therefore, for a desired glass thickness h_g=130um, a desired waveguide height h_{LL} = 50um, and angles calculated for 45° turning, an offset of ~238.6um between the two mask openings is required. For the TIR condition to be established to enable symmetry, the index of refraction ratio between the polymer and the contacting medium must satisfy the following criterion:

$$\frac{n_3}{n_4} \le \sin\theta_2 \tag{5.4}$$

where n_4 is the refractive index of contacting medium. For the proposed set up, the contact medium is air which has a refractive index of $n_4 = 1$. For the given waveguide material and expected angle, the TIR condition is established.

5.4.2 Process Flow

The process flow for the double-sided mask fabrication and the exposure augmentation for the proposed modified inclined lithography process is presented in Figure 5.9. The detailed process steps for the out-of-plane optical turning structure are detailed in Table 5.3.

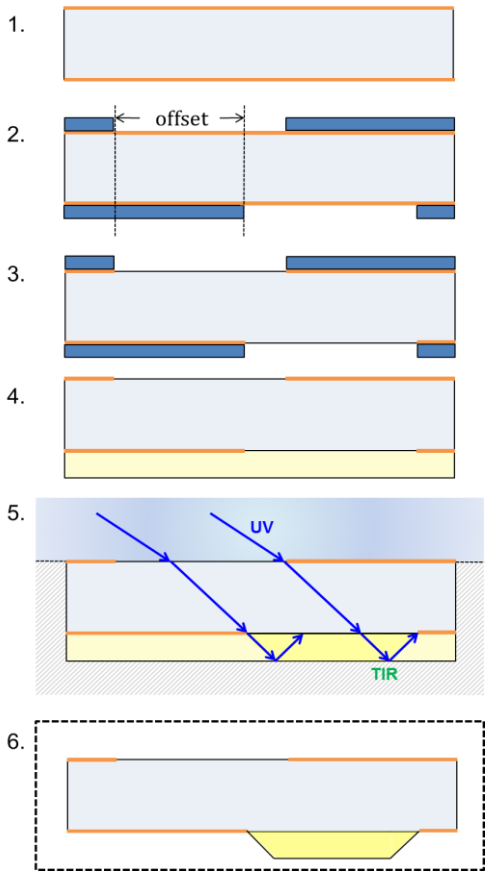

Figure 5.9: Process flow for modified inclined lithography

Table 5.3: Detailed process steps and parameters for optical turning structure fabrication

Process Step	Type	Parameters
1 Metallization	Cu sputter	PVD
2 PR deposition & UV litho.	Roller lamination I-line	125°C 60mJ/cm^2
3 PR stripping & Metal etching	Spray Differential Spray	PR Stripper, 35°C CupraEtch™
4 WG depositon	See Table 4.1	See Table 4.1
5 Inclined litho.	Immersion (I-line)	400mJ/cm^2
6 PEB, Develop & Cure	See Table 4.1	See Table 4.1

Copper was selected as the mask material due to its opacity at i-line wavelengths and in house fabrication experience for fine feature sizes. The copper deposition was performed using PVD sputtering. The masks were fabricated on the substrate with front to back side alignment using an USHIO-44101 projection tool. The polymer waveguide material is processed according to the steps outlined in Chapter 4.1. However, during the exposure step, the substrate and coated polymer were inserted in a holder enabling the required tilt and index-matching media presented by Figure 5.10.

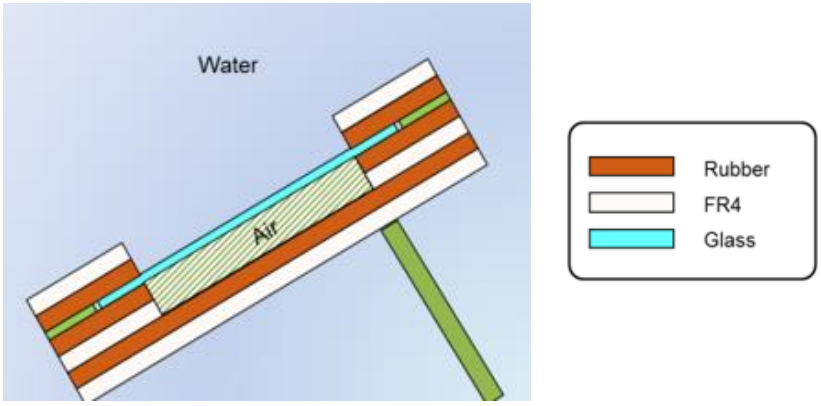

Figure 5.10: Design for holder enabling tilt and index-matching media

5.5 Fabrication Results

Location accuracy of the optical turning structure is the primary objective for validation of the proposed process. Therefore, double sided copper masks were fabricated and optimized for front-to-back alignment and minimal line edge roughness. In addition to location alignment, as with any optical device, low loss must also be ensured. As discussed in the previous section, the required turning angle for 0.5dB loss without an optical via is between 43 and 46 degrees. Therefore, the holder depicted in Figure 5.10 was constructed for variable substrate tilt, and optical turning structures were fabricated and optimized for turning angles within the modeled range.

5.5.1 Double Sided Mask Fabrication

For the double sided mask fabrication, 4"x 4" 150um thick Corning Willow™ glass panels were sputtered with a seed layer of Cu. Typically, a Ti-Cu seed layer is sputtered on bare glass for RDL making as the Ti enhances the adhesion between the glass and copper. However for this application, the metallization is temporary and the seed layer adhesion is not critical. Further, wet etching of the Ti increased line edge roughness. The panels were then laminated with a 15um thick, negative-tone Hitachi dry film photoresist. Figure 5.11 presents the roller laminator used for PR lamination.

After lamination, the photoresist was patterned using a USHIO tool, which has front and back cameras for front-to-back alignment. The stage was shifted by the calculated offset (~238.6 um) for the exposure on one side with respect to the other.

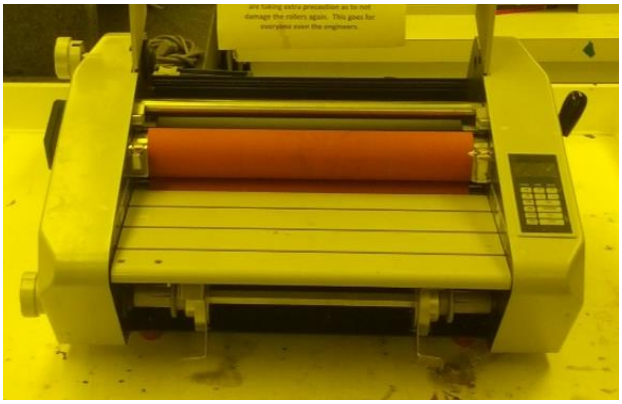

Figure 5.11: DF4200 Roller laminator used for PR lamination

A front-to-back alignment mask misalignment of 1-2 um was measured. Figure 5.12 presents the experimental mask patterned by the USHIO tool. After the fabrication of the double-sided masks, the substrate was prepared according to the parameters described in CHAPTER 3 and siloxane polymer is deposited and processed according to the parameters described in CHAPTER 4.

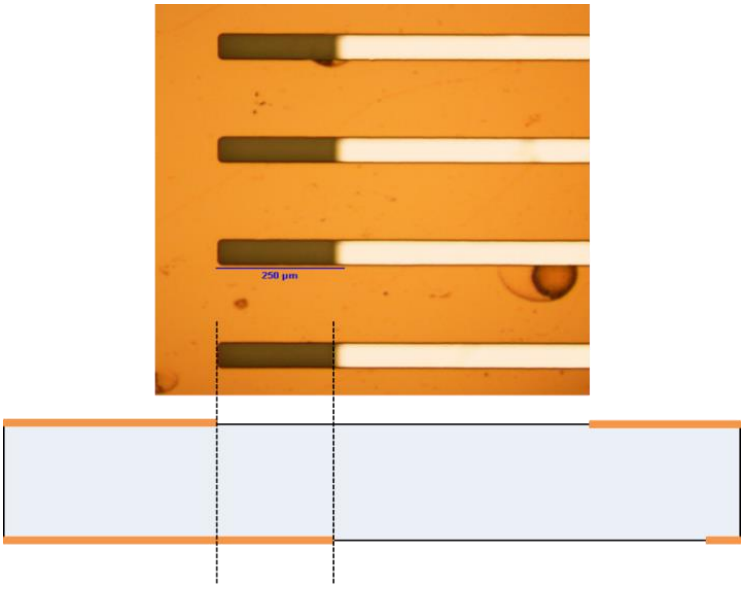

Figure 5.12: Experimental mask offset patterned by USHIO-44101

5.5.2 Substrate Tilt and Turning Angle Control

After the second soft baking, the substrate was ready to for non-planar exposure. Figure 5.13 presents the constructed experimental holder for variable tilt and index-matching media. After being loaded into the experimental holder, the substrate and holder were submerged in water. The placement of the setup into the water caused rippling. Therefore, a 5 min wait after submergence was employed to allow for a smooth water surface. Next, the substrate and holder were flood-exposed using the optimized exposure for the planar case (28s). After exposure, the polymer coated substrate was removed from the holder and a dry air pocket was observed indicating good sealing. Finally, the PEB, development, and curing as described in CHAPTER 4 was performed. A ~57° substrate tilt resulted in the most accurate turning angle (~45°) confirming the tilt calculation. Figure 5.14 presents the fabricated out-of-plane optical turning structure imaged by SEM.

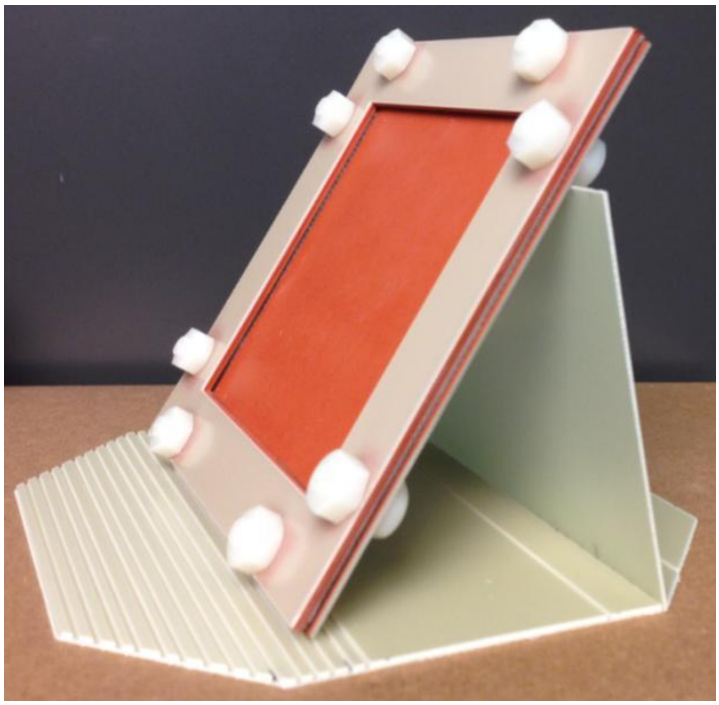

Figure 5.13: Experimental holder for variable tilt and index-matching media

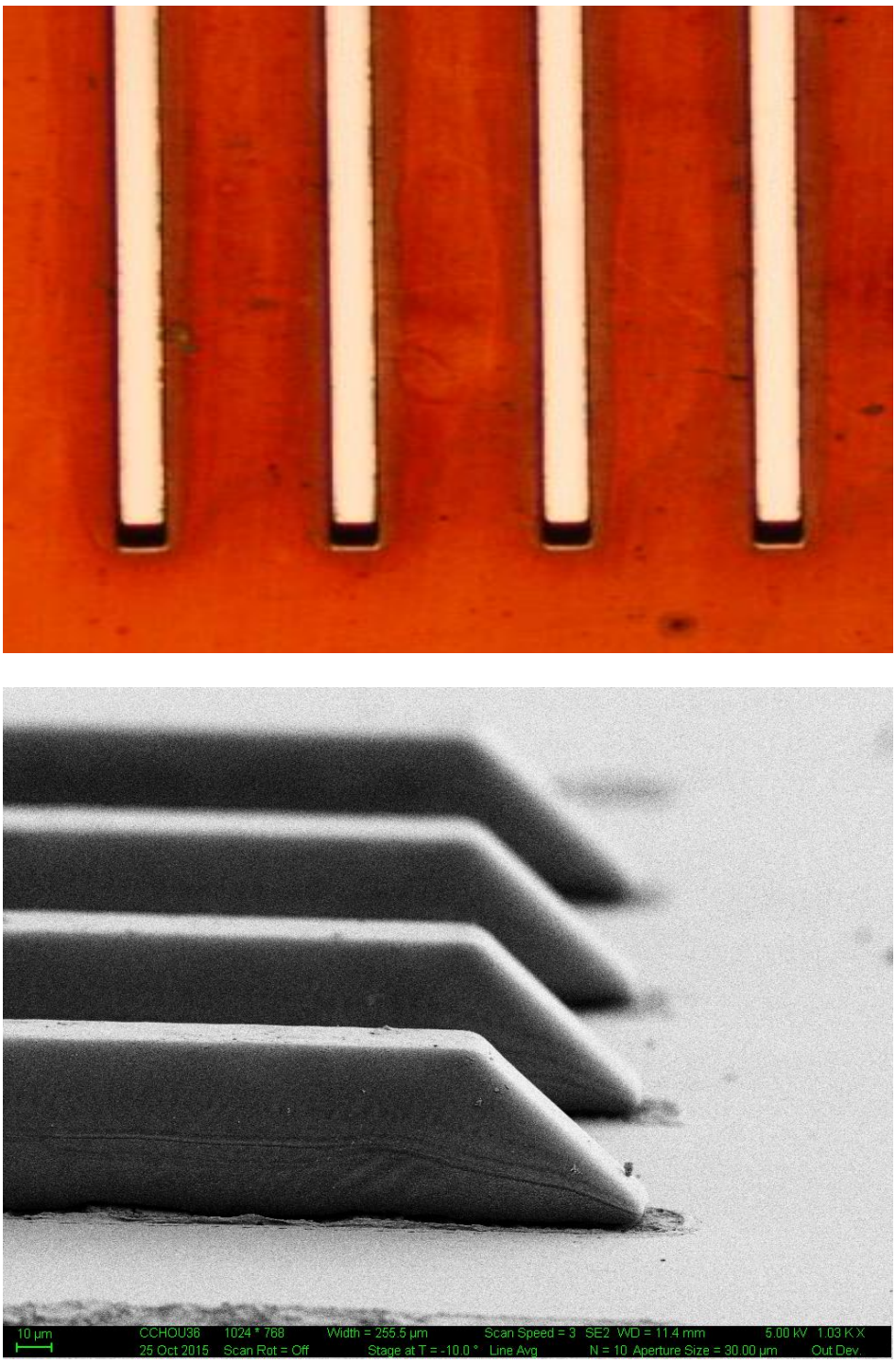

Figure 5.14: Fabricated out-of-plane optical turning structure

5.5.3 Location Accuracy

In order to evaluate the location accuracy, double-sided mask were fabricated with alignment to pre-existing optical vias. The optical vias enabled a reference for each mask and also an assessment of the process compatibility with optical via to be discussed in the next section. The through-vias were drilled by Corning and filled using a novel vacuum-assisted filling process. A multipoint alignment analysis was performed between the optical via and the mask opening. More specifically, sixteen points were inspected and at each point two circles were drawn. One circle outlines the optical via and the other is equidistant between the mask openings. A misalignment vector, $\mathbf{\Delta}$ is defined as the distance between the centers of the two circles.

Figure 5.15 presents the misalignment values at each point and Figure 5.15 presents the methodology for vector measurement, the point mapping across the panel, and the associated misalignment vectors. The average misalignment was ~2.3um and the standard deviation was 1.6um. Combined with the front-to-back misalignment of 1-2 um, this degree of accuracy is suitable for low loss multimode applications. Further, some of the misalignment from this method may be a result of via drift. Therefore, optimization of the via drilling location accuracy and panel-level lithographic accuracies is required for the lowest loss.

Table 5.4: Vector values at each point for multi-point alignment analysis

ID	x (um)	y (um)	|Δ| (um)	ID	x (um)	y (um)	|Δ| (um)
1	0.0	3.6	3.6	9	0.0	0.8	0.8
2	-1.4	4.5	4.7	10	-2.8	0.8	2.9
3	0.0	3.6	3.6	11	-0.5	-0.1	0.5
4	1.4	-2.9	3.2	12	-0.5	1.9	1.9
5	0.9	1.9	2.1	13	0.5	0.5	0.7
6	0.0	0.8	0.8	14	-1.4	-3.4	3.6
7	3.7	-2.4	4.5	15	-0.9	-1.0	1.4
8	0.0	0.8	0.8	16	-0.9	0.3	1.0

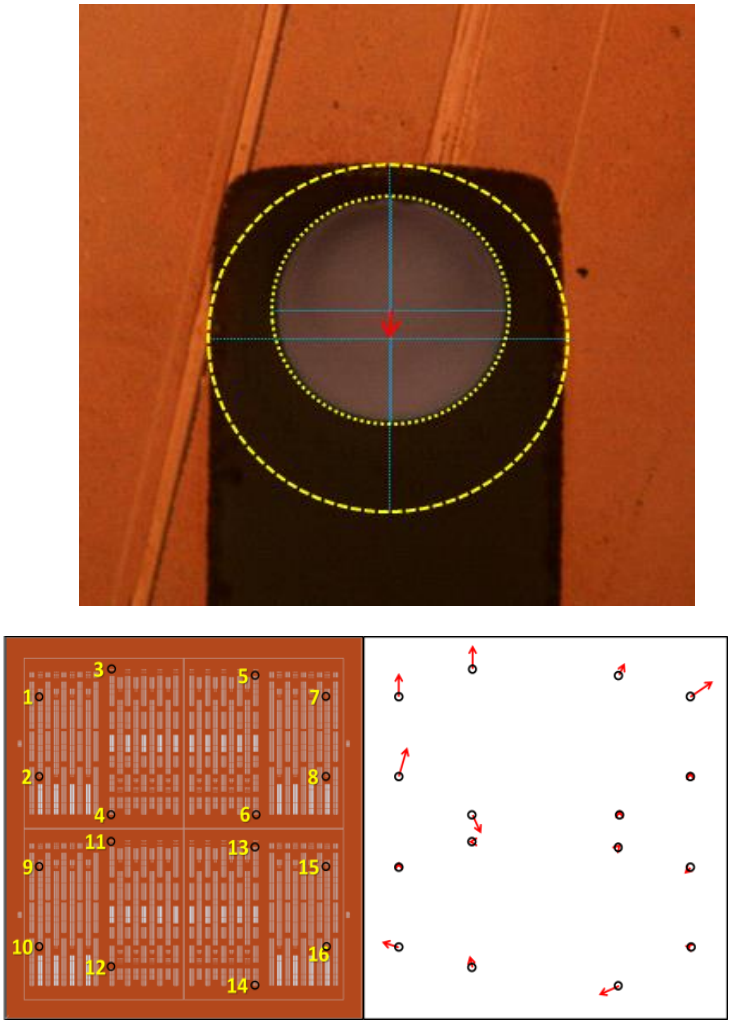

Figure 5.15: Multipoint analysis of location accuracy: (left) single point misalignment vector measurement between optical via and mask opening, (middle) point mapping across panel, (right) associated misalignment vectors

5.6 Process Compatibility With Optical Via

In addition to characterizing the location accuracy, the effect of pre-existing optical vias on turning structure fabrication was characterized. Four cases of turning structure and optical via integration were evaluated on the same panel:

Case 1 has no pre-existing optical vias,

Case 2 has pre-existing optical vias at the entry end,

Case 3 has pre-existing optical vias at the exit end, and

Case 4 has pre-existing optical vias at both ends.

The entry end is defined as the turning end incidentally defined without TIR reflection at the polymer-air interface. For the control case (Case 1), the exit end turning structures were undercut and greater than 45°, indicating insufficient exposure (exposure was not yet optimized during this trial). For cases with pre-existing optical vias at the entry ends (Case 2 and 4), the turning structures were poorly defined. In fact, the turning mirrors and waveguides were deformed due to an undesired ray trajectory as a result of ray effects at the optical via and glass interface with the glass. Scattering likely occurred due to interfacial roughness of the sidewall of the optical via. However, for the case with a pre-existing optical vias at the exit end only (Case 3), the turning structures were defined similarly to Case 1, indicating no effect from the optical vias.

Figure 5.16 presents the polished cross-section of the turning waveguide integrated with a pre-existing optical via at exit end (Case 3). Fortunately, of the pre-existing optical vias,

the entry via is the least critical to total link loss. For light transmitting from the VCSEL, the beam divergence is negligible (1-2°), especially for such a short distance reduced by using ultra-thin glass (150um). For light transmitting from the turning waveguide (modeled in Chapter 5.3), the beam divergence is significant. However, it is recapturable by an optical via – the *exit* optical via as described by Case 3.

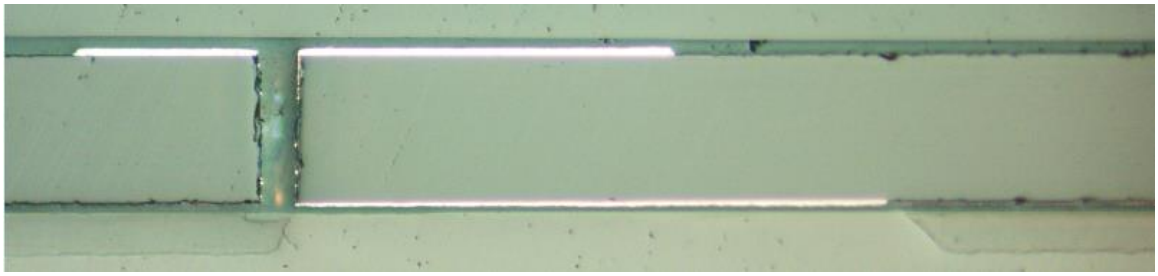

Figure 5.16: Polished cross-section of turning waveguide and optical via

CHAPTER 6

SUMMARY AND FUTURE WORK

This chapter concludes with a summary of the research conducted to enable low loss, low cost, high volume out-of-plane optical turning in a 3D glass interposer and recommendations for future work related to this research.

6.1 Summary

System scaling is required to meet the current and future electronic performance demands. Optoelectronic systems enable system scaling at highest bandwidth, and *potentially* lowest power and cost. Manufacturing advancements of low loss optical interconnections are required to fully realize these benefits.

The in-plane nature of optical interconnections and the out-of-plane nature of superior photonic dies has resulted in an optoelectronic packaging trend relying on **optical turning**. Interposers enable alignment improvements further reducing power loss, which reduces cost. Glass as a substrate enables lowest cost by high volume with the best material properties. Polymer waveguide materials are relatively untested for glass and processes for low loss optical turning structure manufacturing are low volume, serial processes with challenges in alignment. A siloxane-based polymer LightLink™ was selected for its low loss; and a novel, high volume turning structure fabrication process based on inclined lithography was designed and demonstrated using the siloxane polymer to address the alignment challenges.

The glass substrate was designed as the part of the waveguide structure, reducing processing steps and integration complexity. The glass surface was characterized using AFM and contact angle goniometry. Various surface treatments were evaluated and alkaline sonication was selected as the best process for surface wettability. Further, various adhesion enhancements were explored and HMDS priming was selected as the best process for siloxane waveguide adhesion and minimal undercutting on glass substrate.

Planar siloxane waveguides were demonstrated on glass substrate using the glass as cladding. Each step of the siloxane waveguide process was analyzed and optimized to enable waveguide geometries with multi-mode dimensions and precise lithographic definition (i.e. vertical and smooth sidewalls). The optical loss of the waveguides was characterized using the cut-back method and an insertion loss of -- dB and a transmission loss of -- dB/cm was measured.

Out-of-plane optical turning structures integrated with the optimized waveguides were demonstrated on glass substrate using the proposed process. Various modeling approaches were evaluated and 2D Finite Domain Time Difference (FDTD) was selected for its accuracy and computation efficiency. Using 2D FDTD, the turning angle tolerance was modeled with and without optical vias. The process for turning structure fabrication was designed and appropriate tilts and masks offsets were calculated using Snell's Law. An experimental holder was designed and demonstrated to enable the required index of refraction media for precise turning angles within the modeled tolerance and turning

structure symmetry, further reducing process steps. The location accuracy of the fabricated, double-sided masks, which directly correlates to the turning structures location accuracy was characterized. A front-to-back mask offset of ~1-2um was measured and a location accuracy of 2.3um was measured across the panel. The optical loss of the turning structure was characterized using the cut-back method and a turning loss of -- dB was measured. The process was assessed for compatibility with pre-existing optical vias and it was determined that the pre-existing optical via must not interfere with the ray transit through-substrate during exposure. However, the optical via of conflict is of least critical importance to the overall optical loss for the multimode application, especially for ultra-thin glass.

6.2 Recommendations for Future Work

The optoelectronic technology developed in this research is not only poised to meet the needs of the communications industry, but also the automotive. Demands for increasing driving autonomy and in-car entertainment are pushing the needs for high bandwidth solutions, exceeding the existing Media Oriented System Transport (MOST) infrastructure. The implementation of active optical cables, specifically multi-mode fibers, and hot-pluggable glass transceivers as depicted in this research has the potential to enable the required bandwidth with improved reliability at an accordable price. In terms of reliability, the glass substrate offers advantages in mechanical stability, thermal insulation, humidity buffering, and compatibility to glass fibers. The matched CTE to photonic dies, which enables improved photonic die assembly also matches the glass fibers improving their location reliability during thermal cycling.

In order for the polymer waveguide to remain a viable interconnection for this platform, the reliability of both the waveguide and turning structure needs to be characterized. Further, a hermetic seal may be necessary to protect the polymer core during operation. Glass-to-glass bonding may be used to add a protective glass layer.

For the turning structure location alignment to be fully utilized, a high accuracy fiber integration strategy needs to be designed and demonstrated on glass substrate. The location accuracy of the mechanical constraints to pre-existing optical vias or vice versa would need to be of similar accuracy as the demonstrated optical turning structure. Various methods of forming mechanical constraints in glass are available including: glass U-groove (by dicing, etching, or ablation) or even embedded Si V-groove. The fiber may also be accurately constrained by polymer blocks. After the construction of the mechanical constraint, the fiber would need to be attached and secured. An index-matching UV adhesive and/or glass-to-glass weld is recommended to secure the fiber. Additionally, the hermetic seal protecting the optical waveguides and turning structures may also be used to secure/seal the optical fibers.

REFERENCES

[1] D. A. B. Miller, "Device Requirements for Optical Interconnects to Silicon Chips," *Proceedings of the IEEE,* vol. 97, p. 20, 2009.

[2] F. E. Doany, C. L. Schow, C. W. Baks, and D. M. Kuchta, "160 Gb/s Bidirectional Polymer-Waveguide Board-Level Optical Interconnects Using CMOS-Based Transceivers," *IEEE Transactions on Advanced Packaging,* vol. 32, p. 15, May 2009.

[3] L. Brusberg, H. Schröder, C. Ranzinger, and M. Queisser, "Thin Glass Based Electro-optical Circuit Board (EOCB) with Through Glass Vias, Gradient-index Multimode Optical Waveguides and Collimated Beam Mid-board Coupling Interfaces," presented at the Electronic Components and Technology Conference, San Diego, CA, 2015.

[4] K. Nieweglowski, L. Lorenz, K.-J. Wolter, and K. Bock, "Multichannel optical link based on polymer multimode waveguides for boardlevel interchip communication," presented at the European Microelectronics Packaging Conference, Friedrichshafen, Germany, 2015.

[5] H. D. Thacker, R. Shafiiha, J. Lexau, and X. Zheng, "Hybrid Integration and Packaging of an Energy-Efficient WDM Silicon Photonic Chip-to-Chip Interconnect," presented at the Electronic Components and Technology Conference, San Diego, CA, 2015.

[6] I. Shubin, X. Zheng, H. Thacker, and S. S. Djordjevic, "All Solid-State Multi-Chip Multi-Channel WDM Photonic Module," presented at the Electronic Components and Technology Conference, San Diego, CA, 2015.

[7] G. Kim, H. Park, J. Joo, and K.-S. Jang, "Single-chip photonic transceiver based on bulk-silicon, as a chiplevel photonic I/O platform for optical interconnects," *Scientific Reports,* vol. 5, p. 11, Jun 2015 2015.

[8] B. C. Chou, S. Razdan, H. Zhang, J. Sun, T. Bowen, V. Smet, *et al.*, "Modeling, Design, and Demonstration of Ultra-miniaturized and High Efficiency 3D Glass Photonic Modules," presented at the ECTC 2014, Orlando, FL, 2014.

[9] T. Dillon, M. Zablocki, S. Shi, and J. Murakowski, "Micromachining of a fiber-to-waveguide coupler using grayscale lithography and through-wafer etch," *Proc. of SPIE,* vol. 6882, p. 10, 2008.

[10] W. S. Zaoui, M. F. Rosa, W. Vogel, M. Berroth, J. Butschke, and F. Letzkus, "Cost-effective CMOS-compatible grating couplers with backside metal mirror

and 69& coupling efficiency," *OPTICS EXPRESS*, vol. 20, p. 6, Nov 29. 2012 2012.

[11] T. Barwicz, N. Boyer, S. Harel, and T. w. Lichoulas, "Automated, Self-Aligned Assembly of 12 Fibers per Nanophotonic Chip with Standard Microelectronics Assembly Tooling," presented at the Electronics Components and Technology Conference (ECTC), San Diego, CA, 2015.

[12] L. Brusberg, H. Schröder, R. Pitwon, and S. Whalley, "Electro-optical Backplane Demonstrator with Gradient-index Multimode Glass Waveguides for Board-to-board Interconnection," presented at the Electronic Components and Technology Conference, Orlando, FL, 2014.

[13] P.-K. Shen, C.-T. Chen, C.-H. Chang, and C.-Y. Chin, "On-Chip Optical Interconnects Integrated with Laser and Photodetector Using Three-Dimensional Silicon Waveguides," presented at the Optical Fiber Communications Conference and Exhibition (OFC), San Francisco, CA, 2014.

[14] J.-F. Seurin, C. L. Ghosh, V. Khalfin, and A. Miglo, "High-power high-efficiency 2D VCSEL arrays " *Proc. of SPIE*, vol. 6908, p. 14, 2008.

[15] B. C. Chou, Y. Sato, V. Sukumaran, J. Sun, and V. Sundaram, "Modeling, Design, and Fabrication of Ultra-high Bandwidth 3D Glass Photonics (3DGP) in Glass Interposers," presented at the Electronic Components and Technology Conference, Las Vegas, NV, 2013.

[16] B. C. Chou, S. Razdan, H. Zhang, and J. Sun, "Modeling, Design, and Demonstration of Ultra-miniaturized and High Efficiency 3D Glass Photonic Modules," presented at the Electronic Components and Technology Conference, Orlando, FL, 2014.

[17] W. Vis, B. C. Chou, V. Sundaram, and R. Tummala, "Self-Aligned Chip-to-Chip Optical Interconnections in Ultra-Thin 3D Glass Interposers " presented at the Electronic Components and Technology Conference, San Diego, CA, 2015.

[18] B. Chou, W. Vis, R. Furuya, V. Sundaram, and R. Tummala, "Modeling, Design, Fabrication, and Characterization of Ultra-high Bandwidth 3D Glass Photonic Substrates," presented at the International Symposium on Microelectronic, Orlando, Fl, 2015.

[19] V. Sukumanan, T. Bandyopadhyay, V. Sundaram, and R. Tummala, "Low-Cost Thin Glass Interposers as a Superior Alternative to Silicon and Organic Interposers for Packaging of 3-D ICs," *IEEE TRANSACTIONS ON COMPONENTS, PACKAGING AND MANUFACTURING TECHNOLOGY*, vol. 2, p. 8, Sep. 2012 2012.

[20] B. Sawyer, B. C. Chou, S. Gandhi, and J. Mateosky, "Modeling, Design, and Demonstration of 2.5D Glass Interposers for 16-Channel 28 Gbps Signaling Applications," presented at the Electronic Components and Technology Conference (ECTC), San Diego, CA, 2015.

[21] B. Chan, H. Lin, C. Carver, and J. Huang, "Organic Optical Waveguide Fabrication in a Manufacturing Environment," presented at the Electronic Components and Technology Conference (ECTC), Las Vegas, NV, 2010.

[22] J. Mao, L. Deng, X. Jiang, R. Ren, and Y. Zhai, "Polymer Waveguide based Hybrid Opto-Electric Integration Technology," *Proc. of SPIE,* vol. 9270, p. 7, Sep 2014 2014.

[23] W. Kam, Y. S. Ong, W. H. Lim, and R. Zakaria, "Laser ablation and waveguide fabrication using CR39 polymer," *Optics and Lasers in Engineering,* vol. 55, p. 4, April 2014 2014.

[24] B. W. Swatowski, C. M. Amb, S. K. Breed, D. J. Deshazer, and W. K. Weidner, "Flexible, Stable, and Easily Processable Optical Silicones for Low Loss Polymer Waveguides," *Proc. of SPIE,* vol. 8622, p. 11, Feb 20 2013 2013.

[25] E. Anzures, R. Dangel, R. Beyeler, and A. Cannon, "Flexible Optical Interconnects Based on Silicon-Containing Polymers," *Proc. of SPIE,* vol. 7221, p. 12, Feb 2009 2009.

[26] V. Prajzler, P. Nekvindová, P. Hyps, and O. Lyutakov, "Flexible Polymer Planar Optical Waveguides," *Radio Engineering,* vol. 23, p. 7, Sep 2014 2014.

[27] (2016). *EpoCore & EpoClad Serien*. Available: http://www.microresist.de/

[28] T. Han, S. Madden, M. Zhang, and R. Charters, "Low Cost Nanoimprinted Polymer Waveguides " presented at the COMMAD, Sydney, SA, 2008.

[29] (2016, Jan 2016). *LIGHTLINK™ Optical Waveguide Materials*. Available: http://www.microchem.com/Prod-Light-Link.htm

[30] T. Y. Hin, "Materials and Processes to Enable Polymeric Waveguide Integration on Flexible Susbtrates," Doctoral of Philosophu, Loughborough University, 2009.

[31] T. A. Anhoj, A. n. M. Jorgensen, D. A. Zauner, and J. Hubner, "The effect of soft bake temperature on the polymerization of SU-8 photoresist," *J. Micromech. Microeng.*, vol. 16, p. 6, July 28 2006 2006.

[32] S. G. Hegde, "Investigation of Optical Loss Changes in Siloxane Polymer Waveguides During Thermal Curing and Aging," Docotr of Philosophy, School of Mechnaical Engineering, Georgia Institute of Technology, Atlanta, Ga, 2008.

[33] C. Zhang, J.-H. Sun, X. Xiao, and W.-M. Sun, "High Efficiency Grating Coupler for Coupling between Single-Mode Fiber and SOI Waveguides," *CHIN. PHYS. LETT.*, vol. 30, p. 4, 2013.

[34] J. Franc, N. Destouches, D. Blanc, and J.-C. Pommier, "High effciency diffraction grating for multimode optical interconnect," *Proc. of SPIE*, vol. 6185, 2006.

[35] H. Korre, C. P. Fucetola, J. A. Johnson, and K. K. Berggren, "Development of a simple, compact, low-cost interference lithography system," *J. Vac. Sci. Technol. B*, vol. 28, p. 5, Dec. 2010 2010.

[36] L. Brusberg, H. Schröder, and R. Erxleben, "Glass Carrier Based Packaging Approach Demonstrated on a Parallel Optoelectronic Transceiver Module for PCB Assembling," presented at the Electronic Components and Technology Conference, Las Vegas, NV, 2010.

[37] N. Hendrickx, J. V. Erps, E. Bosman, and C. Debaes, "Embedded Micromirror Inserts for Optical Printed Circuit Boards," *IEEE PHOTONICS TECHNOLOGY LETTERS*, vol. 20, p. 3, Oct 15 2008 2008.

[38] X. Dou, X. Wang, H. Huang, X. Lin, D. Ding, D. Z. Pan, *et al.*, "Polymeric waveguides with embedded micromirrors formed by Metallic Hard Mold," *Opt. Express*, vol. 18, p. 8, 2009.

[39] T. Lamprecht, "Embedded Micromirrors for Compact Routing of Mulitmode Polymer Waveguides," PhD, University of Twente, Enschede, The Netherlands, 2011.

[40] J. Jeong, K. Chun, J. Kim, and B. Lee, "Simple Alignment Technique for Molding and Transfer of 3D PDMS Structure using the Mechanical Alignment Jig," presented at the IEEE AFRICON, Nairobi, Kenya, 2009.

[41] M. Tokunari, H.-H. Hsu, and S. Nakagawa, "Assembly and Demonstration of High Bandwidth-Density Optical MCM," presented at the Electronic Components & Technology Conference (2015), San Diego, CA, 2015.

[42] A. Chen, V. Chuyanov, F. I. Marti-Carrera, S. Garner, W. H. Steier, J. Chen, *et al.*, "Vertically tapered polymer waveguide mode size transformer for improved fiber coupling," *Opt. Eng.*, vol. 39, p. 10, 2000.

[43] Y. Hirai, Y. Inamoto, K. Sugano, T. Tsuchiya, and O. Tabata, "Moving mask UV lithography for three-dimensional structuring," *J. Micromech. Microeng.*, vol. 17, pp. 199-206, 2007.

[44] Z. Zhu, Z.-F. Zhou, Q.-A. Huang, and W.-H. Li, "Modeling, simulation and experimental verification of inclined UV lithography for SU-8 negative thick photoresists," *J. Micromech. Microenig.,* vol. 18, 2008.

[45] X. Lin, X. Dou, A. X. Wang, and R. T. Chen, "Polymeric waveguide array with 45 degree slopes fabricated by bottom side tilted exposure," in *Proc. of SPIE*, 2011.

[46] S. M. Garner, H. H. Fong, M. He, and P. Cimo, "Flexible glass substrates for display and lighting applications," presented at the Photonics Conference (IPC), Bellevue, WA, 2013.

[47] N. Sahu, B. Parija, and S. Panigrahi, "Fundamental understanding and modeling of spin coating process: A review," *Indian Journal of Physics*, vol. 83, p. 10, April 2009 2009.

[48] M. Mohynihan, C. Allen, T. Ho, L. Little, and N. Pawlowski, "Hybrid Inorganic-Organic Aqueous Base Compatible Waveguide Materials for Optical Interconnect Applications " *Proc. of SPIE,* vol. 5212, p. 11, Nov 2003 2003.